JOURNAL OF
PETROLOGY

OXFORD

Sulphide Sinking in Magma Conduits: Evidence from Mafic–Ultramafic Plugs on Rum and the Wider North Atlantic Igneous Province

Hannah S. R. Hughes[1]*, Iain McDonald[1], Adrian J. Boyce[2], David A. Holwell[3] and Andrew C. Kerr[1]

[1]School of Earth and Ocean Sciences, Cardiff University, Park Place, Cardiff CF10 3AT, UK; [2]Scottish Universities Environment Research Centre, Rankine Avenue, East Kilbride, Glasgow G75 0QF, UK; [3]Department of Geology, University of Leicester, University Road, Leicester LE1 7RH, UK

*Corresponding author. Present address: School of Geosciences, University of the Witwatersrand, Private Bag 3, Wits 2050, Johannesburg, South Africa. Telephone: +27(0) 11 717 6547. E-mail: hannah.hughes@wits.ac.za

ABSTRACT

Ni–Cu–PGE (platinum group element) sulphide mineralization is commonly found in magmatic conduit systems. In many cases the trigger for formation of an immiscible sulphide liquid involves assimilation of S-bearing crustal rocks. Conceptually, the fluid dynamics of sulphide liquid droplets within such conduits is essentially a balance between gravitational sinking and upwards entrainment. Thus, crustal contamination signatures may be present in sulphides preserved both up- and down-flow from the point of interaction with the contaminant. We examine a suite of ultramafic volcanic plugs on the Isle of Rum, Scotland, to decipher controls on sulphide accumulation in near-surface magma conduits intruded into a variable sedimentary stratigraphy. The whole-rock compositions of the plugs broadly overlap with the compositions of ultramafic units within the Rum Layered Complex, although subtle differences between each plug highlight their individuality. Interstitial base metal sulphide minerals occur in all ultramafic plugs on Rum. Sulphide minerals have magmatic δ^{34}S (ranging from –1·3 to +2·1‰) and S/Se ratios (mean = 2299), and demonstrate that the conduit magmas were already S-saturated. However, two plugs in NW Rum contain substantially coarser (sometimes net-textured) sulphides with unusually light δ^{34}S (–14·7 to +0·3‰) and elevated S/Se ratios (mean = 4457), not represented by the immediate host-rocks. Based on the Hebrides Basin sedimentary stratigraphy, it is likely that the volcanic con duits would have intruded through a package of Jurassic mudrocks with characteristically light δ^{34}S (–33·8 to –14·7‰). We propose that a secondary crustal S contamination event took place at a level above that currently exposed, and that these sulphides sank back to their present position. Modelling suggests that upon the cessation of active magma transport, sulphide liquids could have sunk back through the conduit over a distance of several hundreds of metres, over a period of a few days. This sulphide 'withdrawal' process may be observed in other vertical or steeply inclined magma conduits globally; for example, in the macro-dykes of East Greenland. Sulphide liquid sinking within a non-active conduit or during magma 'suck-back' may help to explain crustal S-isotopic compositions in magma conduits that appear to lack appropriate lithologies to support this contamination, either locally or deeper in the system.

Key words: sulphur isotopes; North Atlantic Igneous Province; sulphide sinking; S/Se; crustal contamination

INTRODUCTION

Upper crustal conduits (pipes, dykes and sills) within mafic–ultramafic magmatic systems provide favourable settings for magmatic sulphide genesis, promoted by crustal contamination, resulting in some of the world's largest orthomagmatic Ni–Cu and platinum group element (PGE) deposits. Contamination can trigger S-saturation of the magma, particularly if the country rocks contain significant amounts of S in the form of sulphides or sulphates; this can be recognized by S isotope signatures outside the typical mantle range of $0 \pm 2‰$ (e.g. Ohmoto & Rye, 1979; versus Li *et al.*, 2002; Ripley *et al.*, 2003; Keays & Lightfoot, 2010; Hayes *et al.*, 2015; Smith *et al.*, 2016). In addition, sulphide liquid that ponds within conduits can become enriched in chalcophile elements, possibly to economic levels, as a result of interaction with magma continuing to pass through the conduit (e.g. Kerr & Leitch, 2005; Holwell *et al.*, 2014).

Sulphides within conduits commonly occur as massive to semi-massive accumulations and are present as rounded globules or droplets of varying sizes; for example, at Norilsk–Talnakh, Russia (Czamanske *et al.*, 1992), the Insizwa Complex, South Africa (Lightfoot *et al.*, 1984), Voisey's Bay, Canada (Huminicki *et al.*, 2008), a mafic dyke in Uruguay (Prichard *et al.*, 2004) and in East Greenland macrodykes (Holwell *et al.*, 2012). Droplets are generally interpreted to represent sulphide liquid that has been transported upwards, downwards or laterally along the magmatic plumbing system. The fluid dynamics involved in this transport, such as settling rate versus entrainment rate, has been the subject of many recent studies based on both empirical and experimental evidence (e.g. de Bremond d'Ars *et al.*, 2001; Mungall & Su, 2005; Godel *et al.*, 2006, 2013; Barnes *et al.*, 2008; Chung & Mungall, 2009; Arndt, 2011).

Sulphide- and chromitite-bearing ultramafic units hosting platinum group minerals (PGM) are documented within the British Paleogene Igneous Province (BPIP) on the islands of Skye, Mull and Rum (Hulbert *et al.*, 1992; Butcher *et al.*, 1999; Pirrie *et al.*, 2000; Power *et al.*, 2000; Prout *et al.*, 2002) and highlight the potential for PGE mineralization in the Scottish portion of the North Atlantic Igneous Province (NAIP; Andersen *et al.*, 2002). This is especially the case considering the potential for contamination offered by the thick crustal sequences of Mesozoic S-bearing rocks in the region (e.g. Hesselbo & Coe, 2000; Yallup *et al.*, 2013; Hughes *et al.*, 2015). Recent studies on Skye demonstrate the involvement of sediments, with light S isotope tenors, in triggering S-saturation in ascending BPIP magmas, particularly in vertical dyke swarms (Hughes *et al.*, 2015). On Rum, ultramafic, vertical or steeply inclined volcanic plugs (pipes) intrude a variety of country rocks, including sediments at the base of the Mesozoic Hebrides Basin. Power *et al.* (2003) identified a crustal $\delta^{34}S$ signature for intercumulus (net-textured) sulphides

in one volcanic plug in NW Rum, but could not establish whether the sulphide liquids that formed these had been entrained upwards or had sunk through the conduit.

In this study, we use the whole-rock S-isotope composition, and sulphide-specific (*in situ*) S-isotope and trace element compositions, of ultramafic plugs on Rum to constrain if crustal contamination took place. The size range and textural associations, trace element composition of sulphide minerals and S-isotopic composition are established for 12 plugs on the island to understand the provenance of sulphide liquids in these conduits. We use these data to decipher controls on sulphide accumulation and compare plug sulphide compositions with those from peridotitic cyclic units of the Eastern Layered Series, part of the Rum Layered Suite. Where crustal contamination is evident [e.g. in NW Rum, as first discovered by Power *et al.* (2003)], these data are combined with numerical modelling of settling and entrainment rates to investigate the roles of magma entrainment and gravitational settling and sinking of sulphide liquids within conduit systems and to assess the distances that sulphide liquids could sink and over what timescale. We provide new constraints on the development of orthomagmatic Ni–Cu–PGE mineralization in small BPIP intrusions and discuss these in relation to wider processes of sulphide migration within magmatic systems.

REGIONAL GEOLOGICAL SETTING

The North Atlantic Igneous Province (NAIP) formed after the impingement of the Icelandic mantle plume under thick continental lithosphere, during a period of continental flood basalt magmatism (e.g. Saunders *et al.*, 1997). Magmatism initiated *c.* 62 Ma within what is now the UK, Greenland and Baffin Island, and ultimately led to the opening of the Atlantic Ocean (Saunders *et al.*, 1997). The main products of this prolonged period of magmatism were tholeiitic and alkali basalts. The British Palaeogene Igneous Province (BPIP) is part of the earliest magmatic series of the NAIP, which includes Palaeogene rocks in the Hebrides and along the west coast of Scotland and Northern Ireland (Saunders *et al.*, 1997; Fig. 1).

In Scotland, the BPIP includes magmatic rocks on the Isles of Mull, Skye and Arran, the Small Isles (Rum, Eigg, Muck, Canna and Sanday), and on the mainland at Ardnamurchan and Morvern (Emeleus & Bell, 2005). The Scottish BPIP extends across a number of Archaean and Proterozoic basement terranes (e.g. Emeleus & Bell, 2005), covered by Neoproterozoic (Dalradian and Moine) metasediments (Kinnaird *et al.*, 2007), which themselves are overlain by Mesozoic sediments from the Hebrides Basin (Hesselbo & Coe, 2000). Volcanic plugs occur within or close to lava fields and central intrusive complexes, and are primarily exposed on the Isles of Mull and Rum (Emeleus & Bell, 2005). Emeleus & Bell (2005) provided a detailed review of
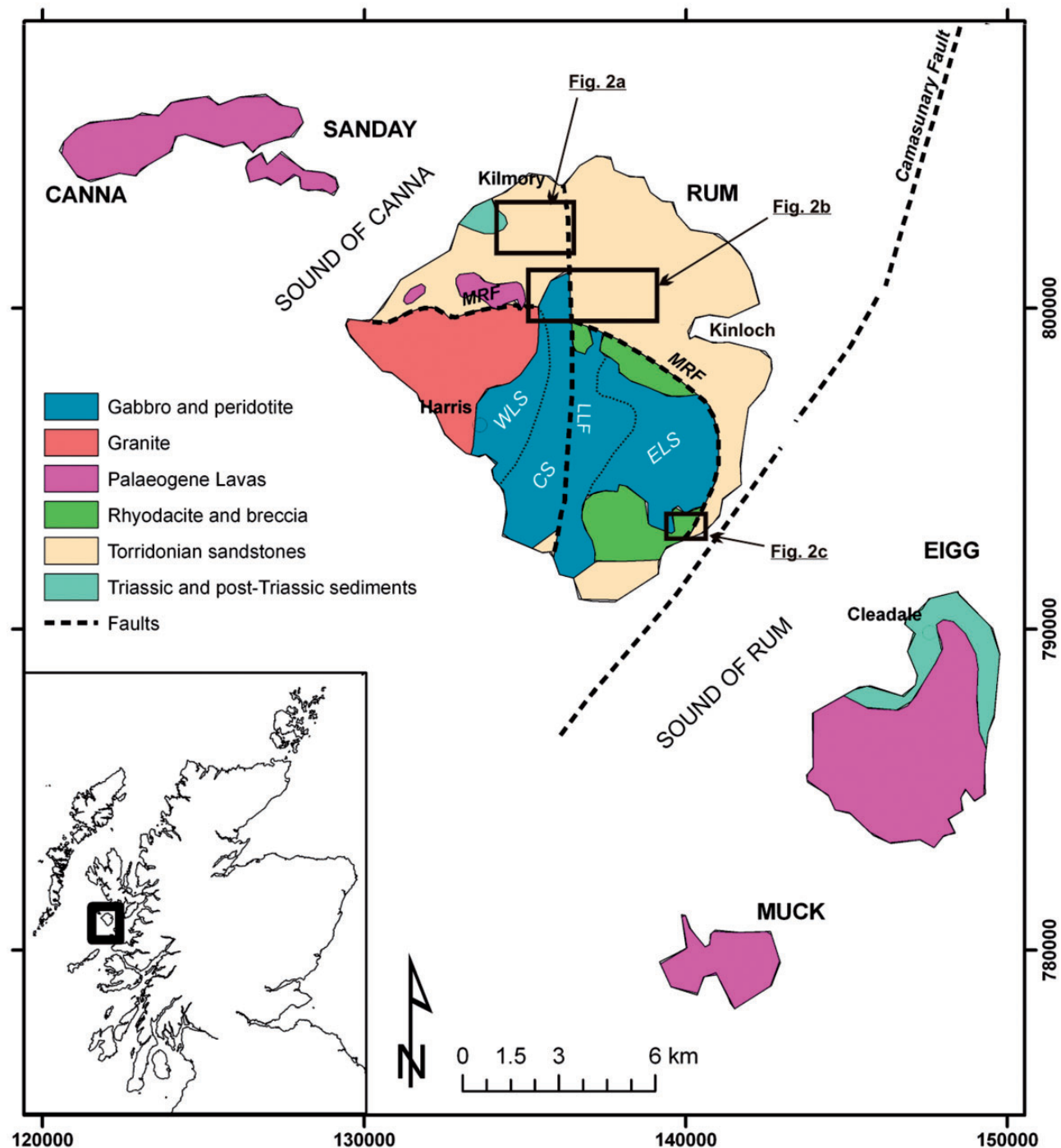
Fig. 1. Simplified geology of the Isle of Rum and surrounding Small Isles. Inset shows outline map of Scotland. Rectangles show map locations in Fig. 2. LLF, Long Loch Fault; MRF, Main Ring Fault; WLS, Western Layered Series; CS, Central Series; ELS, Eastern Layered Series.

radiometric and palynological age determinations of various intrusions and lavas across the BPIP.

Geology of the Isle of Rum

The Rum Central Complex straddles the Long Loch Fault (Fig. 1), which probably acted as a crustal lineament that facilitated magma ascent (e.g. Upton *et al.*, 2002). The complex developed during at least three magmatic phases, forming in < 500 kyr (Emeleus & Bell, 2005; Troll *et al.*, 2008).

In Phase 1, silicic magmatism occurred along an arcuate fault system (the Main Ring Fault) at 60.33 ± 0.21 Ma (Troll *et al.*, 2008) followed rapidly by Phase 2, which formed the mafic–ultramafic Rum Layered Suite (60.53 ± 0.04 Ma; Hamilton *et al.*, 1998).

Ultramafic magmas were intruded into the complex as multiple intrusions and replenishment of the chamber with picritic magma is thought to have disrupted previously formed cumulate layers (e.g. Bédard *et al.*, 1988). The mafic–ultramafic Rum Layered Suite can be divided into the Western, Central and Eastern Layered Series, bounded by the Main Ring Fault (Fig. 1). Rare late-stage picrite dykes [described by Upton *et al.* (2002)] may represent feeders to the layered suites. However, the small melt fraction (6–7%) inferred to have formed these mildly alkalic dykes and two olivine phenocryst populations observed within single picrite dykes, such as M9 (e.g. Upton *et al.*, 2002), preclude these feeders from representing a parental magma composition. During Phase 3, deep subaerial erosion and unroofing of the complex followed caldera collapse and intermittent burial by basalt flows from the Skye lava field (Chambers *et al.*, 2005).

Ultramafic plugs of the Isle of Rum

In excess of 40 volcanic plugs occur on Rum, comprising gabbros and feldspathic peridotite intrusions (*senso stricto* olivine melagabbros) probably formed during Phase 2. Plugs predominantly intrude through Torridonian and Triassic sediments, as well as portions of the Rum Layered Suite (McClurg, 1982; Wadsworth, 1994; Holness, 1999). The sedimentary host-rocks of the volcanic plugs (Triassic, Fig. 2a; and Torridonian, Fig. 2a–c) typically appear bleached, fissile and metasomatized. Locality details of the plugs sampled during this study are given in Table 1 (also see Fig. 2a–c).

The plugs have rounded or elongate- to teardrop-shaped outlines (e.g. Fig. 2a). Their plan-view shapes probably result from varying inclinations of conduits intersecting the present-day topography. Plugs sampled during this investigation are distinct from the small 'apophyses' of peridotite within, or straddling, the Main Ring Fault that may predate or be contiguous with the Eastern Layered Series (e.g. Fig. 2b; Butcher *et al.*, 1985; Wadsworth, 1994). None of the plugs have been radiometrically dated, and the timing of their intrusion is based upon cross-cutting field relationships alone. Most of the plugs lie within 1–2 km of the Long Loch Fault (Fig. 1) and range in size from ∼100 to 600 m diameter (McClurg, 1982; Volker & Upton, 1990). The plugs may have fed lava flows, but no associated lavas have been proven (Emeleus & Bell, 2005).

The structural setting and silicate mineralogy of volcanic plugs on Rum has been studied in detail by Volker & Upton (1990), Wadsworth (1994), Holness (1999) and Holness *et al.* (2012). Ultramafic plugs are thought to represent the conduits of olivine-rich melts or 'crystal mushes', fed from an underlying magma chamber along faults such as the Long Loch Fault. These crystal mushes were lubricated by interstitial basaltic magma, hence the contemporaneous series of gabbroic plugs on the island could represent similar conduits without the entrained olivine mush. Rare plugs in the south of

Rum contain rounded troctolite, dunite and chromitite xenoliths, probably derived from part of the Rum Layered Suite (Volker & Upton, 1990).

Plagioclase (10–15 modal %) and clinopyroxene (up to 8%, sometimes poikilitic) are interstitial to cumulus olivine and euhedral and rounded Cr-spinel; accessory amphibole and biotite are also observed (Wadsworth, 1994). Layering (defined by olivine cumulates) is recorded in the ultramafic peridotite plugs and typically dips shallowly at the margins (striking parallel to the margins) with the central portions of plugs taking on a colloform texture. Changes in modal mineralogy can also define layering, now weathered to 'indentation layering'. At the West Sgaorishal plug (Fig. 2a, Plug 1) indentation layering is particularly well developed and is observed to be closely spaced at the margins (5–10 cm), dipping inwards towards the plug centre at 30–50°, with layer spacing increasing towards, and ultimately disappearing, at the centre. In this plug, olivine accounts for 55–60 vol. % of the rock, but olivine abundance increases to 88 vol. % at the centre. In detail, there is a marked asymmetry in the olivine content from west to east, such that olivine is more concentrated on the western edge (see Holness *et al.*, 2012). In contrast, layering can be poorly developed, laterally discontinuous (e.g. Loch Sgaorishal plug; Fig. 2a, Plug 2) or completely absent in other plugs. Overall, layering developed after magma flow had ceased and/or during magma withdrawal back into the feeder system [compare 'withdrawal' of magmas in Hawaiian conduits, as suggested by Upton (2004)].

Olivine compositions in plugs are equivalent to those from feldspathic peridotites in the Eastern Layered Series (Fo$_{89–82}$) and Western Layered Series (Wadsworth, 1994; Emeleus, 1997, and references therein; Holness *et al.*, 2012) and distinct from olivine compositions in the troctolite portions of the Rum Layered Suite (Fo$_{84–70}$; Emeleus, 1997, and references therein).

The sedimentary host-rocks of the volcanic plugs (Triassic, Fig 2a; Torridonian, Fig. 2a–c) typically appear bleached, fissile and metasomatized. Studies of *in situ* anatexis of country rocks (e.g. Holness, 1999; Holness *et al.*, 2012) and thermal modelling of the West Sgaorishal plug (Plug 1; Fig. 2a) suggest that the plugs were active magma conduit for only a few months and cooled over a period of *c.* 30 years (Holness *et al.*, 2012).

The Hebridean sedimentary succession and country rocks to the Rum plugs

The crustal sequence on the Isle of Rum includes Archaean basement rocks of the Lewisian Gneiss Complex, Mesoproterozoic Torridonian sediments, and Triassic sediments in NW Rum. A thick sequence of Jurassic and Cretaceous sediments probably also covered the island (at least in part), as suggested by extensive outcrops of these rocks preserved on the neighbouring Isle of Skye and 'wedges' of Jurassic
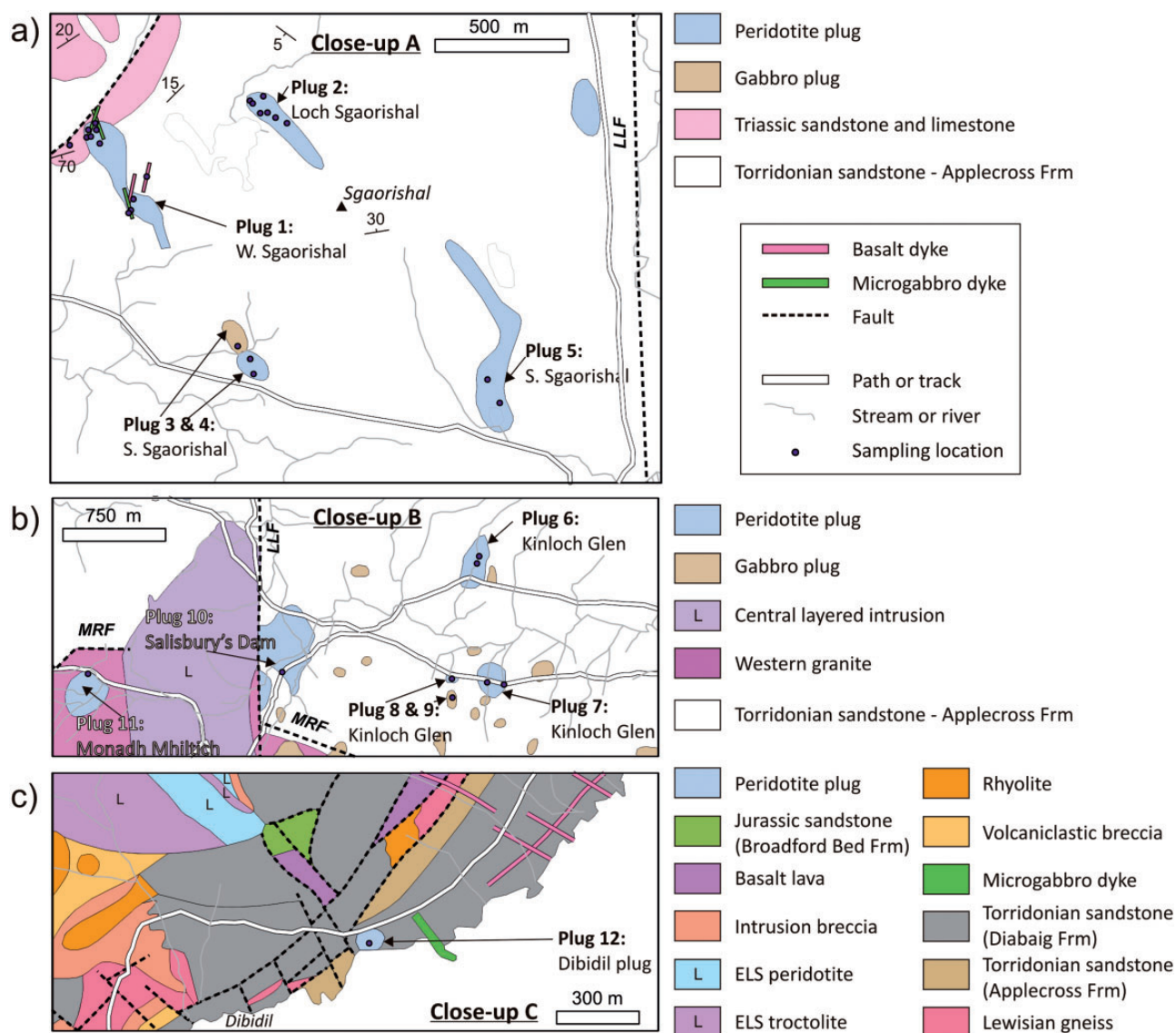
Fig. 2. Geology of areas surrounding the peridotite and gabbro plugs sampled during this study. (a) NW Rum; (b) central Rum across the Long Loch Fault; (c) SE Rum near Dibidil. Sample locations are shown as dots. Plugs are numbered and correspond to Table 1.

mudrocks preserved in the Main Ring Fault of the Rum Central Complex (Emeleus, 1997; for stratigraphic log see Hughes *et al.*, 2015).

S isotope signatures in western Scotland

Lewisian gneisses generally have variable but low sulphur concentrations [median 789 ppm according to Cameron (1994)] and $\delta^{34}S$ ranging from −1·4 to +5·5‰ on the NW Scottish mainland (Lowry *et al.*, 2005; Hughes *et al.*, 2015). The Neoproterozoic Dalradian and Moine metasedimentary successions (Grampian and Northern Highland Terranes, respectively) are mostly dominated by ^{34}S-enriched metasedimentary sequences (Lowry *et al.*, 2005). Moine metapelites have low or very low concentrations of sulphur, and where measurable have $\delta^{34}S = +2\cdot5‰$ (Hughes *et al.*, 2015)

and +3·4 to +4·6‰ in some psammites (Lowry, 1991). Dalradian metasediments (with disseminated diagenetic and metamorphic sulphides, mostly pyrite and pyrrhotite) have a mean $\delta^{34}S$ of +8‰ (±14‰; Lowry *et al.*, 2005).

The Mesoproterozoic Torridonian formations of NW Scotland include the Stoer, Sleat and Torridon Groups (Stewart, 2002; Kinnaird *et al.*, 2007); however, the Stoer Group is thought to be absent on the Isles of Skye and Rum (Figs 1 and 2). Mudrocks are present within the Sleat (and, to a lesser extent, Torridon) Group; however, they are less extensive and thinner than the Jurassic mudrocks of the Hebrides Basin. Sulphur isotope studies of Torridonian sulphates and sulphides in Stoer Group mudrocks have identified the light isotopic shift of $\delta^{34}S$ associated with bacterial sulphate reduction in small freshwater pools (Parnell *et al.*, 2010,

Table 1: Isle of Rum sample information for volcanic plugs and associated sediments

Sample number	Location	Feature type	Plug number (Fig. 1)	Layering
Isle of Rum volcanic plug and associated dyke samples				
RM81	Dibidil	peridotite plug centre	12	none observed
RM58	Kinloch Glen	peridotite plug margin	7	olivine alignment
RM59	Kinloch Glen	peridotite plug centre	7	none observed
RM60	Kinloch Glen	gabbro plug margin	9	none
RM61	Kinloch Glen	peridotite plug centre, homogeneous but heavily weathered with some fresher nodules	8	none observed
RM63	Kinloch Glen	peridotite plug centre	6	none observed, fissile, hydrothermally altered
RM64	Kinloch Glen	peridotite plug centre	6	none observed
RM17	Monadh Mhilitch	peridotite plug margin	11	none observed
RM18	Salisbury's Dam	peridotite plug margin	10	
RM35	Loch Sgaorishal	peridotite plug centre	2	weak layering—olivine alignment
RM70	Loch Sgaorishal	peridotite plug NW margin (at contact)	2	weak layering—olivine alignment
RM71	Loch Sgaorishal	peridotite plug NW margin (5 m inwards from contact)	2	weak layering—olivine alignment
RM73	Loch Sgaorishal	peridotite plug centre	2	weak layering—olivine alignment
RM74	Loch Sgaorishal	peridotite plug NE margin	2	weak layering—olivine alignment
RM75	Loch Sgaorishal	peridotite plug NE margin (~20 m inwards from inferred contact)	2	weak layering—olivine alignment
RM85	Southern Sgaorishal	peridotite plug margin	5	weak cm-scale layering
RM86	Southern Sgaorishal	peridotite plug centre	5	weak cm-scale layering
RM87	Southern Sgaorishal	peridotite plug margin	4	none observed
RM88	Southern Sgaorishal	peridotite plug centre	4	none observed
RM89	Southern Sgaorishal	gabbro plug S margin (~3 m inwards from inferred contact)	3	none
RM29	West Sgaorishal	peridotite plug N margin (~30 m inwards from inferred contact), banded (dipping inwards)	1	indentation layering
RM30	West Sgaorishal	peridotite plug centre, banded and colloform	1	indentation layering
RM32	West Sgaorishal	peridotite plug NW margin (~35 m inwards from inferred contact)	1	indentation layering
RM33	West Sgaorishal	peridotite plug N margin, banded (dipping inwards)	1	indentation layering
RM91	West Sgaorishal	peridotite plug S margin, banded	1	indentation layering
RM95	West Sgaorishal	peridotite plug NW margin, banded (dipping inwards)	1	indentation layering

Sample number	Location	Period: Group, Formation	Sediment type	Sediment sample relationship to volcanic plugs or other proximal magmatic rocks
Isle of Rum sedimentary samples as possible contaminants of plugs				
RM21	Monadh Dubh	Triassic: New Red Sandstone Supergroup, Monadh Dubh Sandstone Formation	conglomerate with calcrete matrix	fresh, but cross-cut by series of cm-scale basaltic dykes and sills
RM22	Monadh Dubh	Triassic: New Red Sandstone Supergroup, Monadh Dubh Sandstone Formation	coarse red sandstone	fresh, but cross-cut by series of cm-scale basaltic dykes and sills
RM23	Monadh Dubh	Triassic: New Red Sandstone Supergroup, Monadh Dubh Sandstone Formation	white limestone	fresh, but cross-cut by series of cm-scale basaltic dykes and sills
RM24	Monadh Dubh	Triassic: New Red Sandstone Supergroup, Monadh Dubh Sandstone Formation	micaceous red arkose	fresh, but cross-cut by series of cm-scale basaltic dykes and sills
RM26	Monadh Dubh	Triassic: New Red Sandstone Supergroup, Monadh Dubh Sandstone Formation	limestone with calcretes	fresh, but cross-cut by series of cm-scale basaltic dykes and sills

(continued)

Table 1: Continued

Sample number	Location	Period: Group, Formation	Sediment type	Sediment sample relationship to volcanic plugs or other proximal magmatic rocks
RM28	Monadh Dubh	Triassic: New Red Sandstone Supergroup, Monadh Dubh Sandstone Formation	limestone	fresh, but cross-cut by series of cm-scale basaltic dykes and sills
RM94	West Sgaorishal	Triassic: New Red Sandstone Supergroup, Monadh Dubh Sandstone Formation	limestone	~60 m from plug margin, limestone is baked
RM3	Guirdil, Isle of Rum	Mesoproterozoic: Torridon Group, Applecross Formation, Scresort Sandstone Member	medium–coarse sandstone	no plugs in vicinity, some small-scale basaltic dykes
RM5	Guirdil, Isle of Rum	Mesoproterozoic: Torridon Group, Applecross Formation, Scresort Sandstone Member	medium–coarse sandstone	no plugs in vicinity, some small-scale basaltic dykes
RM69	Kinloch Glen	Mesoproterozoic: Torridon Group, Applecross Formation, Scresort Sandstone Member	medium–coarse sandstone	unbaked, but ~10 m distance from dolerite sill
RM76	West Sgaorishal	Mesoproterozoic: Torridon Group, Applecross Formation, Scresort Sandstone Member	medium–coarse sandstone	<10 m from Loch Sgaorishal plug margin, baked appearance (grey, fissile)
RM78	Papadil	Mesoproterozoic: Torridon Group, Aultbea Formation, Sgor Mhor Member	sandstone (with heavy mineral bands)	unbaked, fresh-looking sample
RM82	Dibidil	Mesoproterozoic: Torridon Group, Diabaig Shale Formation, Laimhrig Shale Member	shale	Sediment appears partially baked as proximal to S margin of layered intrusion, but still with minor pyrite
RM90	West Sgaorishal	Mesoproterozoic: Torridon Group, Applecross Formation, Scresort Sandstone Member	medium–coarse sandstone	At plug margin, baked, fissile and with evidence of in situ melting (spherules)
RM97	South shore of Loch Scresort	Mesoproterozoic: Torridon Group, Applecross Formation, Allt Mhor na h-Uamha Member	fine sandstone	Unaltered sample, no proximal magmatic features

2012). Hughes *et al.* (2015) established a whole-rock δ^{34}S range of $+1\cdot4$ to $+4\cdot7$‰ for Mesoproterozoic Torridonian sediments on Skye and Rum. They also found that these rocks contained low concentrations of sulphur ($<0\cdot018$ wt %).

The stratigraphy of the Triassic to Cretaceous rocks of the Hebrides Basin is well correlated (e.g. Morton & Hudson, 1995; Hesselbo & Coe, 2000, and references therein) and the S concentration of this Mesozoic sequence is generally much greater than that of the older Torridonian sediments, Moinian metasediments, or crystalline basement (Hughes *et al.*, 2015). Therefore the Mesozoic Hebrides Basin represents the most effective source of crustal S available for magmatic contamination. Sulphur isotopes for Mesozoic (specifically Jurassic) sediments have been reported by Raiswell *et al.* (1993) and Hudson *et al.* (2001) from elsewhere in the British Isles, but Hughes *et al.* (2015), together with results from Yallup *et al.* (2013), have provided the first detailed Hebridean S-isotopic framework.

In summary, Jurassic mudrocks and ironstones have the highest S abundance in the Hebrides Basin, with δ^{34}S ranging from $-33\cdot8$ to $-14\cdot7$‰ (Hughes *et al.*, 2015). δ^{34}S generally becomes lighter from the Lower Jurassic ($-18\cdot4$ to $-14\cdot7$‰) to the Upper Jurassic ($-33\cdot8$ to $-29\cdot2$‰), although the ironstones in the Lower Jurassic (e.g. Raasay Ironstone Formation) generally have the highest bulk S content (up to *c.* 28 wt %, in comparison with some Upper Jurassic shales with 0·1 wt %). In contrast, sediments of the Triassic and Cretaceous succession have volumetrically very few mudrocks and no ironstones, and are therefore less likely to act as major crustal S sources (Hughes *et al.*, 2015). Triassic sediments from Rum (sandstones, conglomerates, breccia and cornstone of the Monadh Dubh Formation) and the wider Hebrides Basin contain calcretes—thus if S were to be present in these rocks, it would most probably be present as sulphate with a heavy δ^{34}S composition (e.g. Power *et al.*, 2003).

Magmatic sulphide mineralization and S contamination in the NAIP

On the Isle of Rum, disseminated and net-textured coarse sulphides (up to 5% modal abundance; Power *et al.*, 2003) occur in the West Sgaorishal peridotite plug (Plug 1; Fig. 2a) within a few metres of the margin. Sulphides are most abundant at the plug margin, and become increasingly rare and fine grained towards the centre (Power *et al.*, 2003). Sulphide-rich zones have not been identified in the other plugs on Rum. PGM are associated with sulphides in Plug 1 and include Pt- and Pd-tellurides, bismuth-tellurides and electrum (Power *et al.*, 2003). Previously reported δ^{34}S values of the coarse sulphides in Plug 1 range from $-18\cdot3$ to $-9\cdot2$‰, and suggest that the magmas forming the plug experienced crustal contamination by Jurassic sedimentary rocks (Power *et al.*, 2003). However, given the absence of crustal rocks with low δ^{34}S currently surrounding the

plug, Power *et al.* (2003) suggested that either S contamination took place in a now-eroded parental magma chamber, or Jurassic sediments originally surrounded the plug locally (and have also since been eroded).

Hughes *et al.* (2015) found that for steeply dipping intrusions, such as basaltic dykes, incorporation of bacterially reduced sulphur from wall-rock shales produced δ^{34}S signatures in magmatic sulphides ranging from $-30\cdot7$ to $-2\cdot3$‰, depending on the degree of contamination and the δ^{34}S signature of the local crustal contaminant. In contrast, horizontal picritic sills on Skye do not record such crustal contamination and lack the anomalous δ^{34}S (Hughes *et al.*, 2015), indicating that the mechanism by which a conduit intruded the surrounding country rock (vertical or horizontal) and the ambient flow regime within it (i.e. turbulent or non-turbulent) were important factors in the contamination process; for example, a turbulent regime is more likely to result in brecciation of the conduit wall rocks, allowing for more efficient S incorporation into the magma (Robertson *et al.*, 2015).

Magmatic Cu–Ni–PGE–Au sulphide mineralization in the wider NAIP is recorded in a number of settings. The largest deposit is the Au- and Pd-dominant Platinova Reef in the Skaergaard Intrusion, formed through prolonged fractional crystallization that eventually triggered S-saturation (e.g. Bird *et al.*, 1991; Andersen *et al.*, 1998; Holwell & Keays, 2014). In this instance, crustal contamination played no role in the formation of an immiscible sulphide liquid. Mineralization is also found as sulphide globules in small hyperbyssal intrusions, such as the Miki Fjord and Togeda Macrodykes of East Greenland (Holwell *et al.*, 2012). Sulphur isotope analyses identified a strong crustal contribution attributed to pyritic Cretaceous black shales, and therefore in these instances crustal S contamination was the trigger for S-saturation (Holwell *et al.*, 2012).

Overall, if crustal contamination is suspected to be the main cause for S-saturation, the isotopic composition of disseminated sulphide mineralization in magma conduits, such as sills, dykes and plugs, can be used as a vectoring tool towards areas of more massive sulphide mineralization (e.g. Lightfoot *et al.*, 1984; Czamanske *et al.*, 1992; Huminicki *et al.*, 2008; Barnes *et al.*, 2016). Hence understanding the source and location of crustal contamination, and the potential crustal horizon(s) that triggered S-saturation in relation to the prevailing fluid dynamic regime in the magmatic conduit, is a valuable method for targeting sulphide-hosted mineralization up- or downstream within the magmatic plumbing systems.

METHODS

Twenty-six whole-rock samples from 12 volcanic plugs from across the Isle of Rum were sampled for major and trace elements, S isotopes (bulk and *in situ*), and mineralogical investigations (sample details are given

in Table 1; localities are shown in Fig. 2a–c; bulk-rock geochemical data are presented in the Supplementary Material, available for downloading at http://www.pet rology.oxfordjournals.org). Additionally, 15 samples of various Torridonian and Triassic sediments were collected from areas adjacent to the plugs, and elsewhere across the island, to assess the crustal S isotopic framework of the island (Table 1).

Bulk-rock and *in situ* S-isotope analysis

For samples with visible sulphide minerals $>500\,\mu m^2$, polished blocks were subjected to sulphide *in situ* laser combustion, following Wagner *et al.* (2002). Raw *in situ* $\delta^{34}S$ data were corrected by the factor $\delta^{34}S_{pyrite} = \delta^{34}S_{SO2laser} + 0.8‰$, as laser combustion causes a small and predictable fractionation of sulphur isotope compositions for the SO_2 gas produced, compared with the actual $\delta^{34}S$ of the sulphide mineral (Wagner *et al.*, 2002). At the Scottish Universities Environment Research Centre (SUERC), SO_2 gases released by combustion were analysed on a ThermoFisher Scientific MAT 253 dual inlet mass spectrometer (conventional samples) and VG Isotech SIRA II mass spectrometer (for laser samples).

Samples without sufficiently large sulphides underwent whole-rock chemical S extraction by the chromium reducible sulphur method (CRS) followed by conventional sulphur analysis: a detailed description and evaluation of this method has been given by Hughes *et al.* (2015). In summary, CRS is based on and adapted from the techniques of Zhabina & Volkov (1978), Canfield *et al.* (1986), Tuttle *et al.* (1986), Hall *et al.* (1988), Newton *et al.* (1995), Nielsen & Hanken (2002) and Labidi *et al.* (2012). Powdered rock samples were loaded into a flat-bottomed glass reaction vessel under a nitrogen atmosphere and connected to a gas bell jar containing $0.1\,M$ $AgNO_3$ solution. A $1M$ solution of chromous chloride ($CrCl_2$) was injected through a septum to cover the powdered sample and was heated to $150°C$ for 3 h to react as follows:

$$2Cr^{2+} + S^0 + 2H^+ \rightarrow 2Cr^{3+} + H_2S.$$
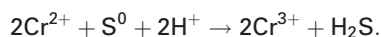
This process leads to the complete breakdown of elemental and reduced sulphur species into H_2S, even in the presence of Fe^{3+}. H_2S produced is streamed to the gas bell jar to react with $AgNO_3$ solution, precipitating Ag_2S. At the end of the reaction, this black precipitate was filtered under vacuum, freeze dried and collected ready for conventional S analysis. During conventional analysis, SO_2 gas samples were run at SUERC using a ThermoFisher Scientific MAT 253 dual inlet mass spectrometer.

Reproducibility for both the laser combustion and conventional analysis is $\pm 0.4‰$ (see Hughes *et al.*, 2015) with 2σ of standards $<\pm 0.2‰$. Standards used throughout all analyses were IAEA-S-3 (–31·5‰) and NBS-123 (sphalerite, $+17.1‰$) international standards,

alongside an SUERC laboratory chalcopyrite standard, CP-1 (–4·6‰).

Bulk-rock S concentrations were determined using a LECO CS230 Carbon/Sulphur Determinator at the University of Leicester. Sample mass ranged from 0·1 to 1·0 g depending on relative bulk S content. Each sample was run in triplicate to monitor precision. Accuracy was monitored by regular analysis of the reference material BAS ECRM 877-1. The limit of minimum detection for this method is 0·018 wt % S (3 × standard deviation of the mean blank).

Mineralogy and mineral composition

Quantitative microanalysis was carried out on a Cambridge Instruments S360 scanning election microscope (SEM), using an Oxford Instruments INCA Energy energy-dispersive X-ray spectroscopy (EDX) analyser, with operating conditions set at 20 kV and specimen calibration current of ~2 nA at a fixed working distance of 25 mm. Analytical drift checks were carried out every 2 h using a Co reference standard and a comprehensive suite of standards from MicroAnalysis Consultants Ltd were used to calibrate the EDX analyser.

Sulphide trace element concentrations were determined by laser ablation inductively coupled plasma mass spectrometry (LA-ICP-MS) using polished samples and a New Wave Research UP213 UV laser system attached to a Thermo X Series 2 ICP-MS system, following procedures outlined by Prichard *et al.* (2013) and Smith *et al.* (2014). Further details are available in the Supplementary Material.

As part of our study, we also analysed the sulphide compositions of a selection of peridotites from each of the major cyclic units in the Eastern Layered Series (ELS), to place plug compositions into context. The results are presented in Table C of the Supplementary Material, alongside whole-rock $\delta^{34}S$ for corresponding ELS samples (Tables D and E, Supplementary Material).

RESULTS

Sulphide mineralogy and trace element compositions

Details of the mineralogy, including size, texture and mineral association of base metal sulphides in the Rum plugs are presented in Table 2 together with a record of any PGM present. SEM-based PGM searches were carried out only on samples from Plugs 1, 2 and 10, as previous work had identified a correspondence between sulphide and PGM occurrences (e.g. Power *et al.*, 2003). As our study focuses on the S-isotopic composition of the plugs and trace element compositions of base metal sulphides within the plugs, we did not undertake a comprehensive search for PGM across all plug samples. Selected back-scattered electron (BSE) images of sulphide mineral textures are shown in Fig. 3.

With the exception of plugs 1 and 2, all the peridotite plugs contain small sulphide blebs (e.g. Fig. 3a),

Table 2: Sulphide mineralogy, texture and grain size.

Sample number	Sulphide minerals	Sulphide size range	Sulphide textures and associations	Silicate and oxides	PGM categories (if detected)	PGM sizes and associations	Other accessory minerals noted
RM18	$Cp + Pn + Po$	$< 20\,\mu m$	Very rare rounded sulphides are interstitial to (but adjacent/in contact with) cumulus olivine crystals	Olivine, clinopyroxene, plagioclase, chromite (also as rare discontinuous veins)	none detected	-	Ni-arsenides, Ni-sulphide (nickeline?), Cu-sulphide (chalcocite?), monazite, apatite, magnetite
RM30	$Po + Pn + Cp$	$< 200\,\mu m$	Sulphides are generally interstitial to cumulus olivine, but much more rare than in RM 32, RM33, RM91. Sulphides usually in contact with olivine at the crystal margins.	Olivine, clinopyroxene, plagioclase, chromite, ilmenite	not investigated	-	White vein cross-cuts sample, filled with serpentine and chlorite, minor quartz
RM32	$Cp + Po + Pn \pm Bo, Cc$	Two size groups: $< 200\,\mu m$, and 0.5 to 4.0 mm	Abundant coarse (0.5 - 4 mm) sulphides as net-textured phases, interstitial to olivine and chromite cumulates. Irregular-shaped to rounded sulphides within intercumulus plagioclase in vicinity of large net-textured sulphides. Additionally, rounded sulphides ($<$ 200μm) within cumulus olivine marginal areas (not serpentised cracks) or embayed at edges of cumulus olivine crystals, and not in vicinity of net-textured coarse sulphides. Also, small sulphides (also $<$ 200 μm) within serpentine-filled alteration cracks throughout slide.	Olivine, clinopyroxene, plagioclase, chromite, ilmenite, serpentinite	Pd-telluride (merensky-ite), Pd bis-muthide-tellurides	0.5 - 4 μm wide PGM, mostly within sul-phides (Pn, Po or Cp) and some at sili-cate-sulphide mineral boundaries	Co-arsenide
RM33	$Cp + Po + Pn \pm Bo, Cc$	0.5 to 2.0 mm	Abundant coarse sulphides as net-textured phase, interstitial to olivine cumulates. Margins of some of these sulphides have 'variagated' solution textures suggestive of alteration or recrystallisaton. Rarely, elongate sul-phides (up to 0.5mm long) can be seen penetrating cumulus olivine crystals along fractures. Chromite crystals both as cumulate phase and sometimes as	Olivine, clinopyroxene, plagioclase, chromite, ilmenite, serpentinite	Pd bismuthide-telluride, Pt-arsenide (sperrylite), Pt-Sb arsenide	0.5 - 7 μm wide PGM, mostly within sul-phides (Po, Pn and Cp) and some at silicate-sul-phide mineral boundaries	electrum, Pb-telluride

(continued)

Table 2: Continued

Sample number	Sulphide minerals	Sulphide size range	Sulphide textures and associations	Silicate and oxides	PGM categories (if detected)	PGM sizes and associations	Other accessory minerals noted
RM35	Cp + Po + Pn + Ga	50 to 500 μm	Sulphides within interstitial silicate minerals (e.g., pyroxene and plagioclase). Smaller rounded sulphides (typically < 100 μm) in contact with margins of cumulus olivine crystals, and associated with serpentine-filled cracks. Rare rounded sulphides (~50 μm) as inclusions in olivine (although crystals are highly fractured). fine inclusions within granular cumulate olivines.	Olivine, clinopyroxene, plagioclase, chromite, ilmenite, serpentinite	Ir-Pt arsenic sulphide (irarsite-platarsite), Ir-arsenic sulphide (irarsite)	(e.g., Po or Pn - silicate) Very rare PGM typically < 1μm wide and found within Pn.	electrum, zircon, chlorite (as replacement mineral overprinting serpentine)
RM58	Cp ± Po ± Pn	< 50 μm	Rounded rare sulphides, as discrete minerals interstitial to cumulate olivine and chromite, and within interstitial pyroxene and plagioclase. Also within serpentinite-filled cracks at margins of cumulus olivines	Olivine, clinopyroxene, plagioclase, chromite	not investigated	-	-
RM61	Cp + Po + Pn ± Bo	< 50 μm	Rounded rare sulphides, as discrete minerals interstitial to cumulate olivine and chromite, and within interstitial pyroxene and plagioclase. Also within serpentinite-filled cracks through cumulate olivines	Olivine, clinopyroxene, plagioclase, chromite	not investigated	-	-
RM64	Cp + Po + Pn ± Bo	< 150 μm	Sulphides are discrete and interstitial to coarse granular cumulate olivine crystals, and sometimes within olivines themselves.	Olivine, clinopyroxene, plagioclase, chromite	not investigated	-	-
RM70	Cp + Pn ± Po	< 90 μm	Sulphides are discrete interstitial to olivine and chromite cumulate crystals, and within intercumulate pyroxenes and plagioclase	Olivine, clinopyroxene, plagioclase, chromite	not investigated	-	-
RM74	Po + Pn ± Cp	< 80 μm	Sulphides are discrete interstitial to olivine and chromite cumulate crystals, and within intercumulate pyroxenes (and variable chlorite-filled zones in OPX ± apatite)	Olivine, clinopyroxene, plagioclase, chromite, ilmenite, serpentinite	not investigated	-	apatite, Fe-oxide
RM75	Cp + Pn ± Po	< 110 μm	Discrete, rounded sulphides, interstitial to granular cumulate olivines, and within intercumulate pyroxenes and	Olivine, clinopyroxene, plagioclase, chromite	not investigated	-	-

(continued)

Table 2: Continued

Sample number	Sulphide minerals	Sulphide size range	Sulphide textures and associations	Silicate and oxides	PGM categories (if detected)	PGM sizes and associations	Other accessory minerals noted
			plagioclase. Sometimes sulphides at triple junction between cumulate olivine crystals.				
RM81	Cp ± Po ± Pn	< 50 μm	Sulphides are discrete and both interstitial to granular cumulate olivines, and within olivines (close to olivine crystal margin)	Olivine, clinopyroxene, plagioclase, chromite, serpentine	not investigated	-	Fe-oxide, serpentine, and replacement of serpentine by chlorite
RM85	Pn + Cc + Bo	< 40 μm	Sulphides are discrete, rounded, and interstitial to granular cumulate olivines, and within intercumulate pyroxenes and plagioclase	Olivine, clinopyroxene, plagioclase, chromite, serpentine	not investigated	-	Fe-oxide, serpentine, and replacement of serpentine by chlorite
RM91	Cp + Po + Pn	0.2 to 4.0 mm	Abundant coarse sulphides as net-textured, interstitial to olivine cumulates. Also more rounded sulphide phases (up to 0.2 mm diameter) in contact with cumulus olivine margins or as embayments at olivine margins.	Olivine, clinopyroxene, plagioclase, chromite	not investigated	-	-
RM95	Cp + Po + Pn	Two size groups: < 50 μm, and 0.25 to 2.0 mm	Abundant coarse sulphides as net-textured phase, interstitial to olivine cumulates. Rare sulphides filling or partially filling cracks through olivine (± serpentine and Fe-oxides) or as discrete rounded/irregular shaped sulphide crystals (< 50 μm) within cracks.	Olivine, clinopyroxene, plagioclase, chromite, serpentine	not investigated	-	-

Mineral abbreviations: Cp, chalcopyrite; Pn, pentlandite; Po, pyrrhotite; Bo, bornite; Cc, chalcocite; Ga, galena; Ol, olivine; Cpx, clinopyroxene; Px, pyroxene; Pl, plagioclase; Ilm, ilmenite; Chr, Cr-spinel; Serp, serpentine; Fe-ox, iron oxide.
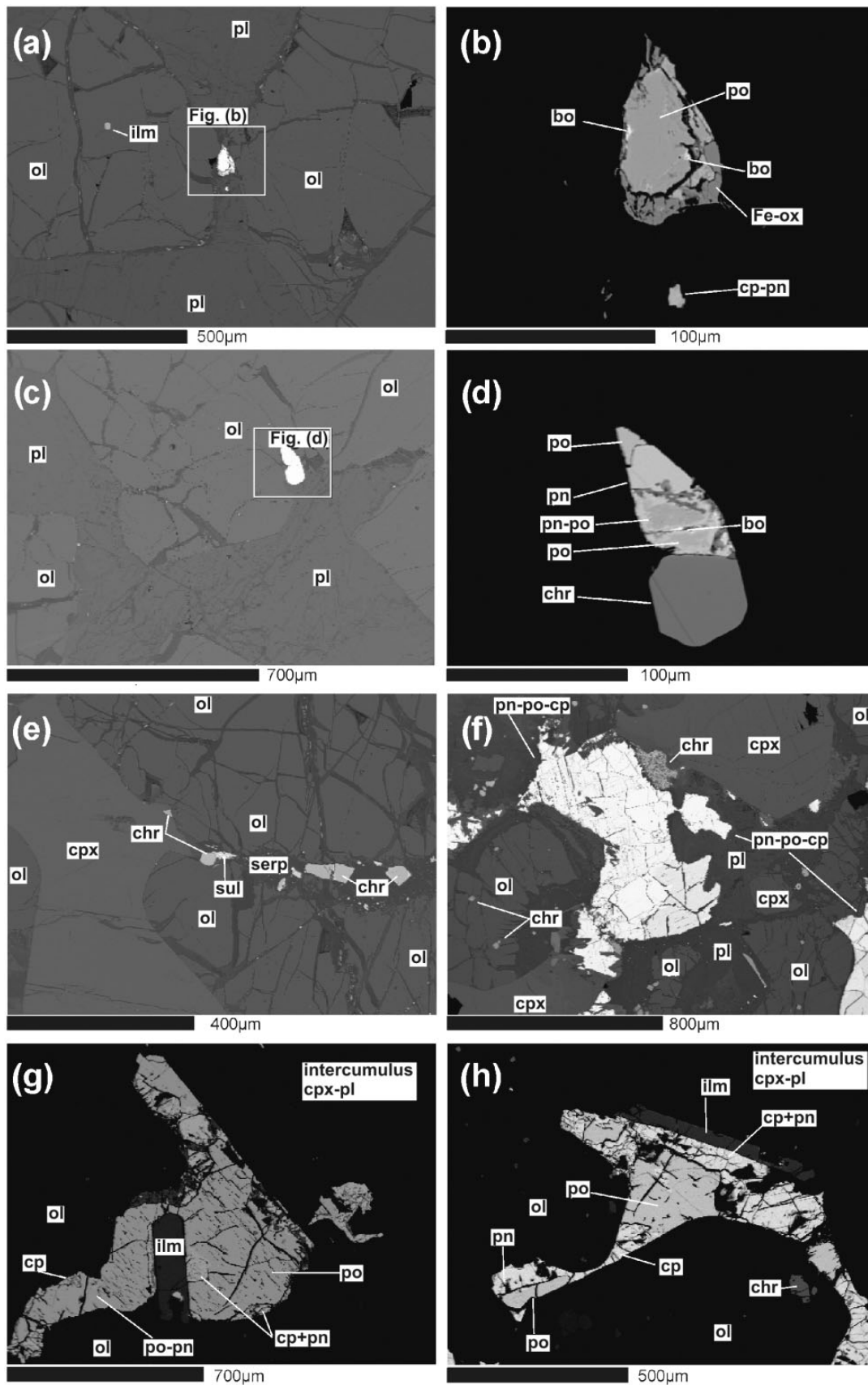
Fig. 3. Back-scattered electron images of sulphides in peridotite plugs from scanning electron microscope investigations. (a) Small sulphide nucleating onto and between two cumulus olivine crystals, within intercumulus plagioclase, plug 6. (b) Close-up of sulphide in (a) with contrast adjusted to show sulphide mineralogy. (c) Sulphide grain nucleating on small Cr-spinel at the margin of granular cumulus olivine, plug 6. (d) Close-up of sulphide minerals and Cr-spinel in (c). (e) Sulphides and Cr-spinel within

typically 20–150 μm in length, rounded and equant, composed of chalcopyrite, pyrrhotite and pentlandite, with rare bornite and chalcocite (Table 2). Occasionally a rim of iron oxide is present around the sulphide blebs in more altered samples (e.g. Fig. 3b). Sulphides normally occur at the margins of cumulus olivine (Fig. 3a and c), or within intercumulus plagioclase and clinopyroxene, and sulphides are locally in contact with granular Cr-spinel (e.g. Fig. 3d). In rare cases, sulphides occur within the fractured and serpentine-filled margins of cumulus olivine (e.g. Fig. 3e). In contrast, plug 1 at West Sgaorishal contains coarser sulphide minerals, up to 4 mm in length, which occur interstitially to pyroxene and plagioclase, or as net-textured assemblages (Fig. 3f–h; Table 2). Sulphides have been observed to almost enclose cumulus olivine, as well as ilmenite and Cr-spinel (e.g. Fig. 3g and h), and include pyrrhotite and pentlandite (and pyrrhotite–pentlandite flames) as well as chalcopyrite. Minor galena is also observed; however, unlike the other plugs, no bornite or chalcocite was encountered in plug 1. Finer sulphide minerals are of the same species as the course sulphides occurring in the centre of plug 1.

PGM (plugs 1 and 2 only) are found within sulphide minerals or at silicate–sulphide mineral contacts. These range in size from 0·5 to 7 μm wide and include Pd- and Pt-tellurides, bismuth-tellurides, Pt-arsenides and Pt–Sb-arsenides (Table 2). In plug 2 (Loch Sgaorishal) sulphides range from 50 to 500 μm and are interstitial to cumulus olivine, with rare rounded sulphides (~50 μm) occurring as inclusions within cumulus olivine, albeit in serpentine-filled fractures. Pentlandite in plug 2 contains small (<1 mm wide) Ir and Pt sulpharsenides of the irarsite–platarsite series. In both plugs 1 and 2, small grains of electrum were observed in pyrrhotite (normally <5 μm) as well as one crystal of Pb-telluride (Table 2).

Representative trace element compositions, including S/Se ratios of sulphide minerals and PGE abundances in plug sulphides (grouped per region of Rum), are presented in Table 3 (full data are available in Supplementary Material Tables C and D). Overall, the variation of PGE concentrations in sulphide minerals from plugs in various areas of Rum (NW, SE and central) overlaps significantly (Fig. 4a–d), such that there is no systematic difference in PGE tenor between plugs. Pentlandite is the principal carrier of Pd but there is no correlation between Pd and Rh for any of the plugs (Fig. 4a), nor are Rh concentrations higher in pentlandite or correlated with Ni content (Fig. 4b). By contrast, Rh and IPGE (Os, Ir, Ru) abundances in pentlandite are not distinct from other base metal sulphides or 'mixed sulphide' analyses (Figs. 5b and d).

The chondrite-normalized PGE composition of coarse sulphides at the margins of plug 1 (Fig. 5a–c) is subtly different from the composition of fine sulphides at the centre (Fig. 5d). This difference is particularly noticeable for Os, Ir and Ru, with the concentration of all PGE in marginal sulphides being lower than in finer sulphides at the centre. Overall, for each type of base metal sulphide (chalcopyrite, pentlandite, pyrrhotite), the sulphide PGE patterns of plug 1 (particularly the margins) are fairly consistent and parallel to one another. However, chalcopyrite (Fig. 5a) generally has lower PGE abundances than pentlandite and pyrrhotite (Fig. 5b and c, respectively), but the overall normalized PGE spectra are similar or parallel between Ni–Fe mineral species (e.g. Fig. 5b and c). Sulphides in plug 2 (Fig. 5e) also have two distinctive PGE patterns, with sulphides at the margin being comparatively homogeneous, and of a similar composition to those from the margin of plug 1. However, two sulphides analysed from the centre of plug 2 have differing PGE compositions—one that overlaps the sulphide compositions of the margins, and one entirely different sulphide composition with notably elevated IPGE. In the instance of plug 2, this may be due to a fundamental difference in sulphide mineralogy, as the sulphide analysed in sample RM35 has a notably lower Cu content (Table 3).

Overall, sulphide compositions from plugs 4–12 are heterogeneous (Fig. 6). This may in part be explained by their being analyses of 'mixed sulphide' species (owing to their small size) but this cannot account for all the observed variation, as even sulphides with comparable Fe, Cu and/or Ni contents fluctuate between plugs. We note that whole-rock geochemistry is similarly variable between these plugs (albeit subtly) (see Supplementary Material). Broadly, peridotite plug sulphide compositions resemble those from peridotite units in the Eastern Layered Series (Fig. 6).

S-isotope compositions and S/Se ratios of the Rum plugs

Figure 7a shows the average $\delta^{34}S$ value for whole-rock samples per plug (data in Table 4, along with S wt %) and for the ELS, plotted against S/Se ratio per sulphide. S/Se was calculated from LA-ICP-MS analyses of Se and calibrated by prior quantitative SEM analyses of S from the same sulphide grain (or in cases of small mixed sulphides a mean stoichiometric S abundance was assumed) and therefore quantifies S/Se on a mineral-by-mineral basis per sample. Sulphide minerals large enough to be analysed by laser combustion (i.e. only in plug 1) on a sulphide mineral-by-mineral basis (Table 5) have been averaged to the mean $\delta^{34}S$ value

serpentinized fracture at margin of cumulus olivine, with intercumulus clinopyroxene, plug 5. (f) Coarse sulphides as a poikilitic phase with clinopyroxene and plagioclase, plug 1 margin. (g) Poikilitic sulphides surrounding cumulus olivine and elongate ilmenite, with intercumulus plagioclase, plug 1 margin. (h) Similar to (g), demonstrating poikilitic, sometimes 'net-textured' sulphides surrounding granular cumulus olivine phenocrysts. In both (g) and (h) the contrast has been adjusted to display the sulphide internal texture and mineralogy. A summary of sulphide characteristics and PGM is presented in Table 2. ol, olivine; cpx, clinopyroxene; pl, plagioclase; ilm, ilmenite; chr, Cr-spinel; serp, serpentine; Fe-ox, iron oxide; pn, pentlandite; po, pyrrhotite; cp, chalcopyrite; bo, bornite.

Table 3: Representative LA-ICP-MS data for plug sulphides

Sample number	Mineral	n	Plug number	Spot or line	S* (wt %)	Se (ppm)	S/Se	Co (ppm)	Ni (wt %)	Cu (wt %)	Zn (ppm)	Os (ppm)	Ir (ppm)	Ru (ppm)
RM30	Sulph (mean)	4	1	spot	36	137	2911	3451	28·09	1·45	1252	3·90	0·35	2·90
RM32	Cp (mean)	2	1	line	35·27	74	4961	290	1·61	23·54	8491	0·08	0·04	<0·09
RM32	Pn	1	1	line	33·38	111	3015	4540	27·59	1·48	466	1·06	0·37	0·84
RM32	Pn–Po (mean)	2	1	line	39·61	79	5067	2200	14·21	2·63	889	0·91	0·19	0·24
RM32	Po (mean)	4	1	line	41·62	104	4054	311	2·51	0·06	99	1·30	0·48	1·02
RM33	Cp	1	1	line	40·78	38	10812	7	0·19	13·36	1804	<0·02	<0·02	<0·09
RM33	Pn (mean)	2	1	line	32·34	53	6120	3440	28·21	0·12	38	1·16	0·25	0·50
RM33	Pn–Po	1	1	line	37·40	31	12128	472	1·96	0·49	36	0·53	0·13	0·13
RM33	Po (mean)	3	1	line	36·39	46	8195	72	0·81	0·16	34	0·52	0·16	0·35
RM91	Cp (mean)	3	1	line	32·03	76	4248	617	5·88	15·41	3778	0·18	0·71	0·54
RM91	Pn (mean)	3	1	line	35·00	113	3094	2493	30·31	0·50	239	2·39	1·10	2·00
RM91	Po (mean)	3	1	line	41·89	111	3827	51	0·61	0·22	1200	1·33	0·61	1·35
RM95	Cp (mean)	2	1	line	33·62	44	7694	298	3·29	28·59	6725	0·02	0·02	<0·09
RM95	Pn (mean)	6	1	line	35·49	76	4878	6121	27·78	1·28	1295	0·49	0·20	0·23
RM95	Po (mean)	2	1	line	39·36	65	6055	191	1·69	0·52	115	0·33	0·07	0·10
RM35	Sulph (mean)	2	2	spot	36	359	1030	3571	25·61	0·23	1529	72·78	21·86	13·84
RM70	Sulph (mean)	4	2	spot	36	237	1721	2260	13·91	6·07	8199	0·68	0·24	1·07
RM75	Sulph (mean)	3	2	spot	36	301	1339	3135	20·12	1·57	907	1·71	0·80	5·32
RM87	Sulph (mean)	3	4	spot	36	137	2885	1064	3·46	7·18	10617	4·25	1·58	3·90
RM85	Sulph (mean)	2	5	spot	36	630	647	6451	36·24	1·11	1203	1·73	0·10	0·10
RM64	Sulph (mean)	4	6	spot	36	292	1450	1621	12·03	8·83	7667	1·52	1·12	2·04
RM58	Sulph	1	7	spot	36	146	2463	1015	8·65	9·19	9124	0·16	0·10	0·14
RM61	Sulph (mean)	3	8	spot	36	240	1539	1876	7·30	13·20	13940	0·40	0·17	0·12
RM61	Po	1	8	line	36·19	34	10530	400	0·76	3·58	6767	0·09	0·02	<0·09
RM18	Sulph	1	10	spot	36	328	1099	805	5·60	8·45	3966	0·50	0·35	0·61
RM81	Sulph (mean)	4	12	spot	36	159	2304	1699	12·00	3·96	4295	1·20	0·13	1·79

Sample number	Rh (ppm)	Pt (ppm)	Pd (ppm)	Au (ppm)	Cd (ppm)	As (ppm)	Bi (ppm)	Te (ppm)
RM30	0·18	0·40	8·92	0·23	6·99	143·58	5·57	43·62
RM32	<0·22	<0·02	0·34	0·02	51·51	<15	0·69	16·63
RM32	<0·22	<0·02	0·59	0·02	10·64	<15	1·29	15·71
RM32	<0·22	<0·02	3·49	0·22	9·64	<15	2·33	4·32
RM32	0·51	<0·02	1·29	0·10	3·88	<15	1·79	10·15
RM33	<0·22	<0·02	0·43	0·03	45·53	<15	0·36	17·35
RM33	0·40	<0·02	22·50	1·87	<1·1	<15	0·31	7·90
RM33	<0·22	<0·02	2·96	<0·01	<1·1	<15	0·60	1·60
RM33	0·29	<0·02	0·25	<0·01	<1·1	<15	0·34	2·96
RM91	<0·22	0·02	6·25	0·02	25·78	20·03	0·61	9·06
RM91	1·16	0·04	40·11	<0·01	1·35	20·42	1·52	21·87
RM91	0·71	0·02	0·98	<0·01	7·42	<15	1·41	11·18
RM95	0·24	<0·02	<0·2	0·04	66·06	<15	2·17	12·42
RM95	0·24	0·06	28·11	0·02	6·01	46·11	1·39	12·17
RM95	<0·22	<0·02	1·02	<0·01	<1·1	<15	1·61	11·15
RM35	1·49	4·79	9·03	0·01	1·25	38·58	5·43	27·39
RM70	0·23	1·14	6·48	<0·01	36·32	54·86	0·64	15·55
RM75	0·70	0·23	8·23	0·07	3·29	36·13	11·33	20·03
RM87	0·42	0·12	0·71	0·03	14·97	16·50	0·33	1·17
RM85	0·13	0·23	13·84	0·06	7·35	637·68	3·28	110·73
RM64	0·74	3·03	46·60	0·04	13·02	<9	1·87	<0·9
RM58	<0·11	<0·02	<0·25	<0·01	2·72	<9	3·59	5·28
RM61	0·12	<0·02	0·61	0·27	15·99	<9	0·24	3·92
RM61	<0·22	0·03	<0·2	<0·01	5·70	<15	<0·05	1·30
RM18	1·78	<0·02	1·24	0·20	8·72	<9	0·59	9·98
RM81	0·18	0·52	2·61	1·64	24·90	27·48	0·48	13·75

*S content of sulphide is from quantitative analyses of the sulphide mineral or assumed as 36 wt % for spot analyses.
(See Supplementary Data Table C for all plug sulphide analyses and Table D for all ELS sulphide data.)

listed in Supplementary Material Table A, so as to be comparable with other samples analysed by whole-rock S extraction and conventional analysis. The $\delta^{34}S$ results of Hughes *et al.* (2015) for various sediments on the isles of Rum and Skye are also shown in Fig. 7b.

The S/Se ratios of ELS samples are mostly outside the mantle sulphide range (2550–3750; Lorand *et al.*, 2003) with only 8% of analyses falling within this range,

84% of analyses being below mantle values (see Supplementary Material Table D). The full range of ELS S/Se ratios is 489–5416 (Fig. 7a) and $\delta^{34}S$ ranges from –4·4 to +1·2‰. Excluding plug 1 and one anomalous value from plug 8, the S/Se ratios of plug sulphides are up to 4000. With the exception of plugs 1 and 2, the peridotite plugs have $\delta^{34}S$ ranging from –0·6 to +2·1‰, in comparison with the ELS peridotites, which range from
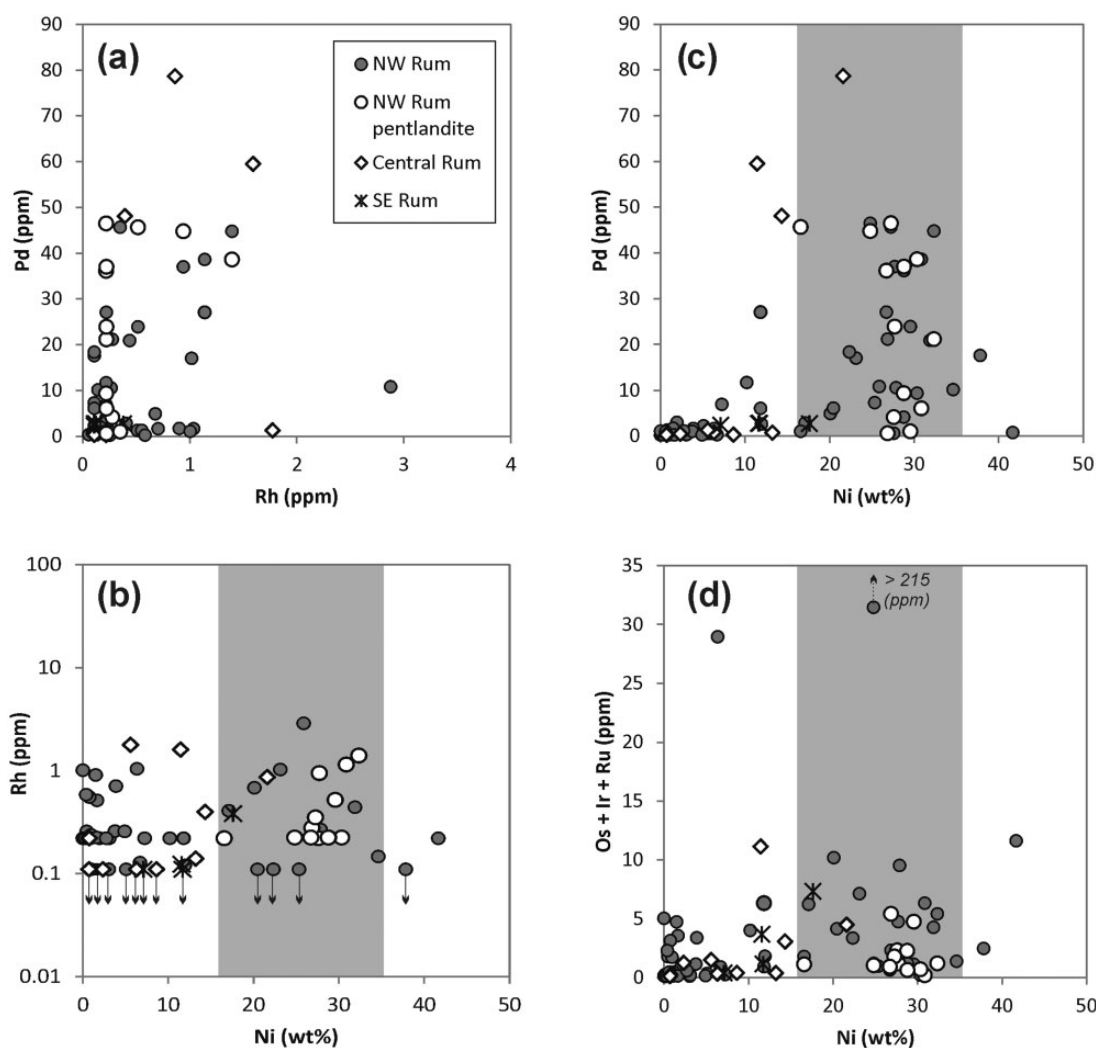
Fig. 4. Trace element variation diagrams for all sulphide minerals analysed by LA-ICP-MS, grouped by area on Rum (NW, Central, and SE). Open circles represent pentlandite where it could visually be recognized and targeted by LA-ICP-MS. This serves to highlight PGE vs Ni abundance for known pentlandite, for comparison with fine sulphide grains where analysis by individual base metal sulphide was not possible, resulting in a 'mixed sulphide' analysis. Grey shaded area in (b)–(d) delineates the pentlandite field (based on a minimum of 17 wt % Ni, assuming a 50:50 mix between pentlandite and pyrrhotite). Note that where PGE abundances were less than the detection limit, results are calculated as half the detection limit and delineated by a small downward arrow.

−1·0 to 0·9‰. Thus, most of the peridotite plug sulphides have $\delta^{34}S$ and S/Se ratios comparable with, and within range of, sulphides from ELS peridotite units. In contrast, sulphides from plug 1 have extremely light $\delta^{34}S$, ranging from −14·7 to −8·0‰, and S/Se ratios ranging from 3000 to 12 000. The centre of Plug 1 shows least variation and deviation of S/Se from the ELS; however, $\delta^{34}S$ is −10·9‰. Whereas the S/Se ratios of plug 2 are within range of the ELS, the $\delta^{34}S$ composition ranges from −6·5 to −2·9‰ (Fig. 7a and Table 4).

DISCUSSION

Magmatic context of the Rum plugs in relation to the Rum Central Complex

The peridotite plugs included in this study have whole-rock major and trace element and PGE signatures that are

subtly distinctive from one another (Supplementary Material Table B) but, broadly, the range of major element compositions overlaps with those recorded for the various portions of the Rum Layered Suite, including peridotite units from the Eastern, Western and Central Layered Series (see Emeleus, 1997; O'Driscoll *et al.*, 2009, and references therein) and the M9 picritic dyke (Upton *et al.*, 2002).

The Layered Suites on Rum are the result of multiple injections of ultramafic magma, in an open magmatic system (e.g. Wager *et al.*, 1960). Current consensus postulates that layering resulted from interaction between cumulates and later magmatic pulses derived from subsequent intruding picrites (e.g. Bédard *et al.*, 1988; Volker & Upton, 1990; Emeleus, 1997; Holness, 2005; O'Driscoll *et al.*, 2007; Leuthold *et al.*, 2014). The S/Se data for the ELS display a broad range from 489 to 5416 (Fig. 7 and Supplementary Material Table D).
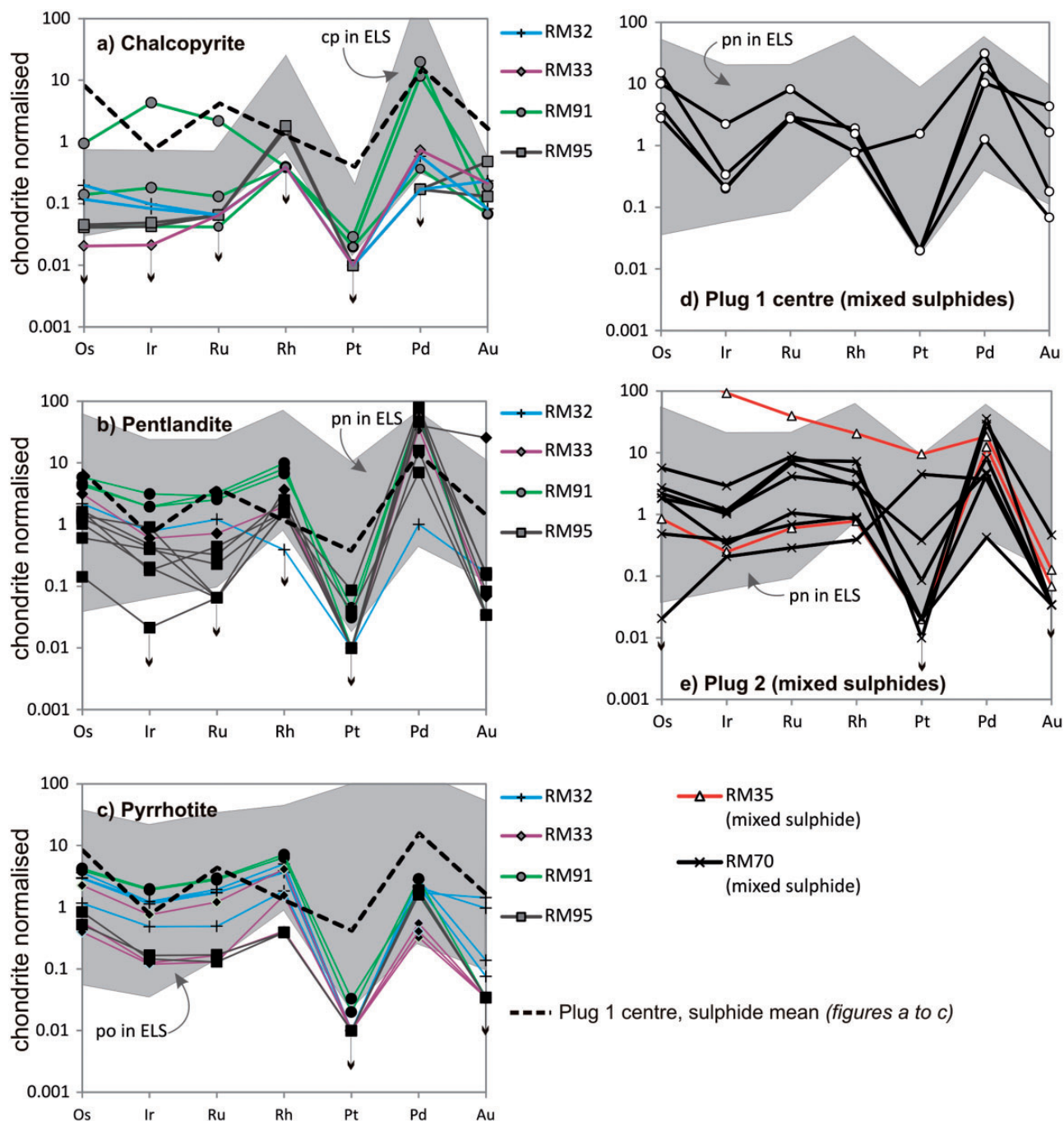
Fig. 5. Chondrite-normalized PGE spectra for sulphide minerals, measured by LA-ICP-MS, for plugs 1 (centre and margin) and 2. Diagrams for analyses from the margin of plug 1 are divided according to sulphide phase: chalcopyrite (a), pentlandite (b), and pyrrhotite (c). Also shown are 'mixed sulphides' in plug 1 [centre; (d)] and plug 2 (e). Normalizing values are from McDonough & Sun (1995). (See Table 3 for summary of data.) It should be noted that where PGE abundances were less than the detection limit, results are calculated as half the detection limit and delineated by a small downward arrow. Grey shaded areas show the range of compositions for chalcopyrite (cp), pentlandite (pn) and pyrrhotite (po) measured in the Eastern Layered Series (ELS; see Supplementary Data Table D) for comparison in plots (a)–(c). Dashed line shows the mean 'mixed sulphide' composition from the centre of plug 1. In plots (d) and (e) the grey shaded area delineates ELS, pn only.

Mantle S/Se ratios typically range from 2550 to 3750 (Lorand *et al*., 2003) and although most of the ELS data are within this range there are significant deviations. Loss of S via oxidation of sulphide minerals will lower the primary S/Se ratio. This is also consistent with the common observation of partially oxidized sulphide minerals in thin sections of the ELS; we suggest that this is the cause of ELS S/Se ratios <2000. In contrast, the causes of an increase in S/Se ratio (i.e. >3750) are two-fold: this can be the result of either hydrothermal mobilization of S, forming a series of hydrothermal sulphide minerals, or contamination of the magmas by
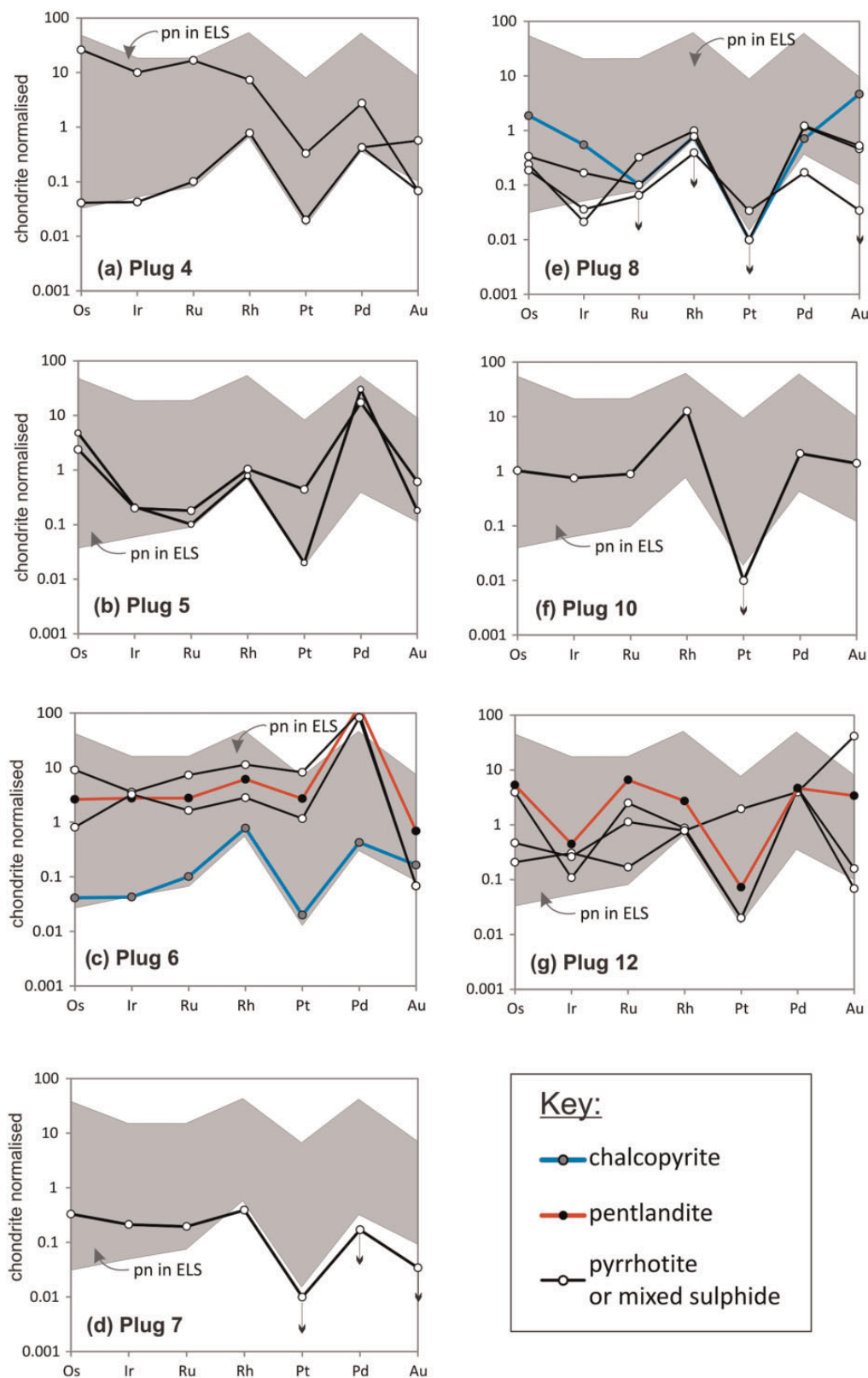
Fig. 6. Chondrite-normalized PGE spectra for sulphide minerals, measured by LA-ICP-MS, for peridotite plugs 4, 5, 6, 7, 8, 10 and 12. Normalizing values from McDonough & Sun (1995). (See Table 3 for details.) It should be noted that where PGE abundances were less than detection limit, results are calculated as half detection limit with small downward arrow. Grey shaded areas delineate range of compositions for pentlandite (pn) in the Eastern Layered Series (ELS) for comparison.
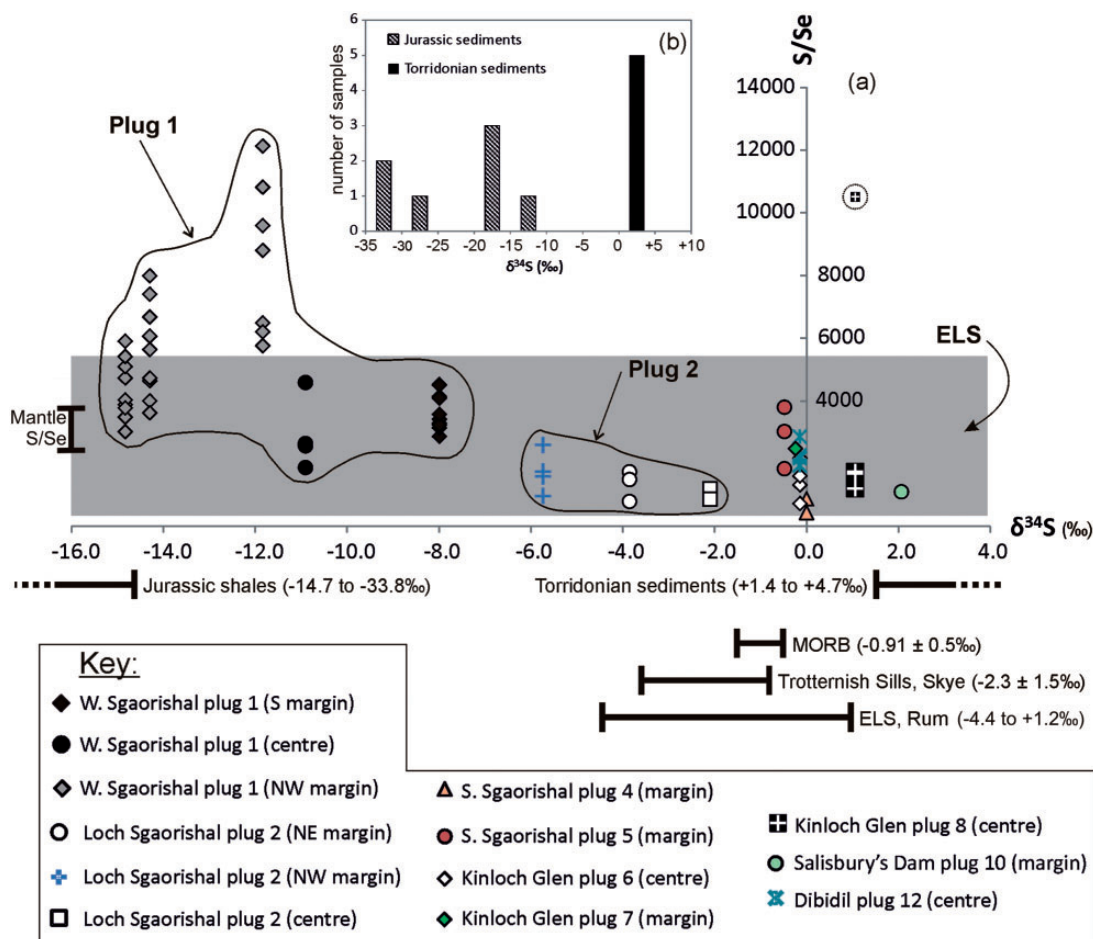
Fig. 7. (a) S-isotope composition (δ^{34}S) vs S/Se ratio of peridotite plug sulphides. Grey shaded area delineates the variation in S/Se ratio for the ELS, and brackets show the range of S/Se for the mantle based on Lorand *et al.* (2003), and δ^{34}S for Jurassic shales, Torridonian sediments and the Trotternish Sills (Isle of Skye) from Hughes *et al.* (2015). MORB δ^{34}S is from Labidi *et al.* (2012). δ^{34}S for the ELS is also shown (see Supplementary Material Table E). (b) Histogram of δ^{34}S for Proterozoic (Torridonian from Rum and Skye) and Mesozoic (specifically Jurassic mudrocks and ironstones from Skye and Ardnamurchan) sediments present in this area of the Hebrides; data from Hughes *et al.* (2015).

crustal S (which is devoid of Se, and thus has a high S/Se ratio). Although δ^{34}S is commonly used as a proxy for crustal S contamination, recent studies suggest that with enough magma throughput in the magmatic (conduit) system, the 'S signal' can be swamped by magmatic δ^{34}S (–2·0 to +0·4‰ for the Iceland plume; Torssander, 1989; and –2·3 ± 1·5‰ for the Isle of Skye picrites; Hughes *et al.*, 2015), whereas the S/Se ratio remains a more reliable proxy for crustal contamination (Ihlenfeld & Keays, 2011).

We record a minimum in δ^{34}S locally in unit 1 (ELS) of –4·4‰, but earlier studies have reported δ^{34}S as low as –14·8‰ in ELS unit 1 rocks with sulphide concentrations locally up to 3 modal % (Faithfull, 1985; Hulbert *et al.*, 1992). These lighter δ^{34}S values occur strictly within unit 1 rocks in the vicinity of metre-scale rafts of Jurassic mudrocks (Faithfull, 1985). In this study, we did not obtain a δ^{34}S composition for the Jurassic mudrock rafts, but we see no reason to disagree with the inference made by Hulbert *et al.* (1992). In general, Hebridean Jurassic mudrocks, including those in

proximity to dolerite and picrite sills on Skye, have a similarly light S-isotopic signature, although those adjacent to intrusions have been significantly degassed owing to contact metamorphism and devolatilization, thereby reducing their bulk S content (Yallup *et al.*, 2013; Hughes *et al.*, 2015). In higher cyclic units in the ELS, δ^{34}S falls within the typical magmatic range; however, sporadic increases in S/Se ratio (>4350) may indicate localized crustal S contamination. This probably took place during intrusion of magmas into the layered suite, and may not be recorded in the δ^{34}S either because of the contaminant having an S-isotopic composition similar to the magma or because high volumes of magma throughput have obliterated the signal. Ultimately, the complexities of sulphide composition, S/Se ratio and S-isotopic composition throughout the ELS and Rum Layered Suite as a whole require further investigation, which is beyond the scope of this study.

The diversity of S/Se ratios and PGE compositions measured in ELS sulphides from our study overlaps with sulphide compositions from the plugs. Therefore

Table 4: Sulphur isotopic composition (δ^{34}S, mean per sample) and whole-rock sulphur concentration

Sample number	Location	Plug no. ([Fig. 1](#))	Plug type	Margin or centre	δ^{34}S (‰)	S (wt %)
RM81	Dibidil	12	peridotite	centre	−0·2	0·03
RM58	Kinloch Glen	7	peridotite	margin	−0·2	—
RM59	Kinloch Glen	7	peridotite	centre	—	—
RM60	Kinloch Glen	9	gabbro	margin	—	—
RM61	Kinloch Glen	8	peridotite	centre	+1·1	—
RM63	Kinloch Glen	6	peridotite	centre	−0·6	—
RM64	Kinloch Glen	6	peridotite	centre	−0·1	—
RM17	Monadh Mhiltich	11	peridotite	margin	N/P	—
RM18	Salisbury's Dam	10	peridotite	margin	+2·1	—
RM35	Loch Sgaorishal	2	peridotite	centre	−2·9	—
RM70	Loch Sgaorishal	2	peridotite	NW margin (at contact)	−5·7	0·05
RM71	Loch Sgaorishal	2	peridotite	NW margin (5 m inwards from contact)	−3·7	—
RM73	Loch Sgaorishal	2	peridotite	centre	−4·2	—
RM74	Loch Sgaorishal	2	peridotite	NE margin	−6·5	0·06
RM75	Loch Sgaorishal	2	peridotite	NE margin (∼20 m inwards from inferred contact)	−3·9	0·03
RM85	Southern Sgaorishal	5	peridotite	margin	—	—
RM86	Southern Sgaorishal	5	peridotite	centre	+0·3	0·02
RM87	Southern Sgaorishal	4	peridotite	margin	−0·5	—
RM88	Southern Sgaorishal	4	peridotite	centre	−1·3	0·04
RM89	Southern Sgaorishal	3	gabbro	S margin (∼3 m inwards from inferred contact)	—	—
RM29*	West Sgaorishal	1	peridotite	N margin (∼30 m inwards from inferred contact)	−11·0	—
RM30*	West Sgaorishal	1	peridotite	centre	−10·9	0·02
RM32*	West Sgaorishal	1	peridotite	NW margin (∼35 m inwards from inferred contact)	−14·7	0·08
RM33*	West Sgaorishal	1	peridotite	N margin	−11·8	—
RM91*	West Sgaorishal	1	peridotite	S margin	−8·0	0·18
RM95*	West Sgaorishal	1	peridotite	NW margin	−14·3	—

Sample number	Location	Period: Group, Formation	Sediment type	δ^{34}S (‰)	S (wt %)
RM21	Monadh Dubh	Triassic: New Red Sandstone Supergroup, Monadh Dubh Sandstone Formation	conglomerate with calcrete matrix	N/P	—
RM22	Monadh Dubh	Triassic: New Red Sandstone Supergroup, Monadh Dubh Sandstone Formation	coarse red sandstone	N/P	—
RM23	Monadh Dubh	Triassic: New Red Sandstone Supergroup, Monadh Dubh Sandstone Formation	white limestone	N/P	—
RM24	Monadh Dubh	Triassic: New Red Sandstone Supergroup, Monadh Dubh Sandstone Formation	micaceous red arkose	—	—
RM26	Monadh Dubh	Triassic: New Red Sandstone Supergroup, Monadh Dubh Sandstone Formation	limestone with calcretes	—	—
RM28	Monadh Dubh	Triassic: New Red Sandstone Supergroup, Monadh Dubh Sandstone Formation	limestone	N/P	—
RM94	West Sgaorishal	Triassic: New Red Sandstone Supergroup, Monadh Dubh Sandstone Formation	limestone	—	—
RM3†	Guirdil, Isle of Rum	Mesoproterozoic: Torridon Group, Applecross Formation, Scresort Sandstone Member	medium–coarse sandstone	+1·4	—
RM5†	Guirdil, Isle of Rum	Mesoproterozoic: Torridon Group, Applecross Formation, Scresort Sandstone Member	medium–coarse sandstone	+3·0	—
RM69	Kinloch Glen	Mesoproterozoic: Torridon Group, Applecross Formation, Scresort Sandstone Member	medium–coarse sandstone	N/P	—
RM76	West Sgaorishal	Mesoproterozoic: Torridon Group, Applecross Formation, Scresort Sandstone Member	medium–coarse sandstone	N/P	—
RM78	Papadil	Mesoproterozoic: Torridon Group, Aultbea Formation, Sgor Mhor Member	sandstone (with heavy mineral bands)	N/P	—
RM82	Dibidil	Mesoproterozoic: Torridon Group, Diabaig Shale Formation, Laimhrig Shale Member	shale	N/P	—
RM90	West Sgaorishal	Mesoproterozoic: Torridon Group, Applecross Formation, Scresort Sandstone Member	medium–coarse sandstone	N/P	—
RM97	South shore of Loch Scresort	Mesoproterozoic: Torridon Group, Applecross Formation, Allt Mhor na h-Uamha Member	fine sandstone	N/P	—

Sulphur isotopic composition was measured via conventional methods (following whole-rock sulphur extraction), except for samples with asterisk.

*Sulphur isotopic composition measured via laser combustion methods (for plug 1 only).

—, analysis was not run for that sample. Detection limit of bulk S is 0·018 wt %. N/P, no Ag_2S precipitate was recovered following bulk-rock sulphur extraction.

we suggest that the plugs (conduits) record various crystal mush injection events broadly coincident with magma (or mush) injections into the Rum Layered Suite. As such, the magma conduits represented by the peridotite plugs were not formed from a single eruption event, and probably represent multiple eruptions.

Feeders and magma staging chamber for the plugs and Rum Layered Suite

The presence of dunite, chromitite, and troctolite xenoliths within peridotite plugs situated inside or close to the Main Ring Fault (Volker & Upton, 1990) suggests that ejection of crystal mushes that fed these plugs occurred whilst crystallization of the layered series was taking place. This demands a physical brecciation of wall-rock material, and does not provide evidence that the conduit crystal mushes were derived from the layered suites directly, but instead indicates that they erupted through them.

One striking observation regarding the Rum plugs is the lack of troctolite plugs. In contrast, feldspathic peridotites (strictly olivine melagabbros) described in our study exist alongside gabbroic plugs that have no phenocryst assemblage or other evidence for their having been intruded as a crystal mush, unlike the peridotite plugs. It is possible that the gabbroic plugs represent the basaltic magmas ejected from a staging magma chamber, and there is no evidence to suggest that these gabbroic plugs correlate strictly with the troctolite portions of units in the Rum Layered Suite. Indeed, per cyclic unit in the Rum Central Complex, the peridotite base and troctolite tops are typically paired in the Eastern Layered Series (Emeleus & Troll, 2011, and references therein; O'Driscoll et al., 2014). Regardless of the mechanism that formed the overall layering of this suite, it is apparent that each of the troctolite layers is a fractionation feature associated and paired with each peridotite layer. Therefore because the peridotitic crystal mush that was ejected through the volcanic pipes is of a comparable composition to the peridotitic bases of the layered suite cyclic units, this suggests that the crystal mushes of both came from a common source, and not necessarily that the layered suites directly fed the plugs themselves. This is supported by the observation that small entrained sulphide minerals in both the plugs and layered suite peridotites are directly comparable with one another (according to both S/Se and $\delta^{34}S$, except for plugs 1 and 2, which are discussed below). In other words, there must have been a separate deeper staging chamber in which a peridotitic crystal mush evolved, before being tapped by the magmatic plumbing system to both the layered suites and the plugs.

The origin of sulphides within the Rum plugs

With the exception of plugs 1 and 2, the sulphide minerals observed are of low abundance and are small, often rounded phases ($<150 \mu m$ in diameter); sometimes these sulphides occur as embayments within cumulus olivine (e.g. Fig. 3c and e, and Table 2). All plugs have distinctive chondrite-normalized PGE and Au patterns and S/Se ratios, some of which closely resemble the compositions of sulphides in peridotite units of the ELS (e.g. Figs 6–8). The Fo content of cumulus olivine in the plugs suggests that previously crystallized olivine phenocrysts were entrained within a basaltic or picritic magma, such that the peridotite plugs were essentially crystal mush conduits (e.g. Wadsworth, 1994; Holness et al., 2012) sometimes with entrained chromitite, dunite or troctolite xenoliths (e.g. Volker & Upton, 1990). We propose a similar scenario for the entrainment of sulphide liquids.

The magmatic temperature of the peridotite plugs on Rum has previously been estimated at 1400°C, based on picritic magma temperatures (Holness et al., 2012). The solidus temperature of an Fe-bearing sulphide liquid is c. 1100°C (Bowles et al., 2011; after Kullerud & Yoder, 1959; Arnold, 1971) suggesting that sulphides would be liquid at the estimated temperature of emplacement for the plugs. Given that the 'lubricating' magmas were energetic enough to entrain up to 50% olivine crystals (e.g. Holness et al., 2012) and sizeable xenoliths (e.g. Volker & Upton, 1990), it is highly likely that these were also capable of entraining immiscible sulphide droplets. A similar scenario of upward sulphide liquid entrainment has been suggested in the vicinity of Grasvally in the Northern Limb of the Bushveld Complex by Smith et al. (2016), suggesting that S-saturation occurred in a deeper master chamber (albeit via deep crustal contamination with a distinctive S-isotopic and S/Se composition). Therefore, we suggest that at least some sulphides (with mantle S/Se ratios) were formed prior to intrusion of the plugs, and were transported as sulphide liquid droplets into these conduits.

Sulphur content at sulphide saturation (SCSS), as defined by Li & Ripley (2005), is dependent upon the bulk composition of the magma (MgO, FeO^T, SiO_2, Na_2O and K_2O), pressure and temperature. Assuming the magmatic temperature of 1400°C from Holness et al. (2012) and using the bulk compositions of gabbroic plugs (e.g. plugs 3 and 9) and ultramafic plugs (e.g. plug 12 at Dibidil, and plug 1 at West Sgaorishal) reported in the Supplementary Material, we find that SCSS would be 2985 ppm (plug 12), 3510 ppm (plug 1) and 1830 ppm for the two gabbroic plugs (plugs 3 and 9) at 1 km depth [using the equation of Li & Ripley (2005)]. For the ultramafic plugs, this is apparently well in excess of the measured bulk S concentration (Table 4). However, we highlight that this bulk concentration potentially incorporates up to 50% cumulus olivine, and therefore the actual S concentration of the interstitial magma carrying the crystal mush will have been significantly higher if this is taken into account (i.e. up to double that measured). Further, a late picrite dyke (M9) on Rum is calculated to reach an SCSS at 1400°C and 1 km depth of 3000 ppm S. Upton et al. (2002) observed up to 60 vol. % olivine phenocrysts and we
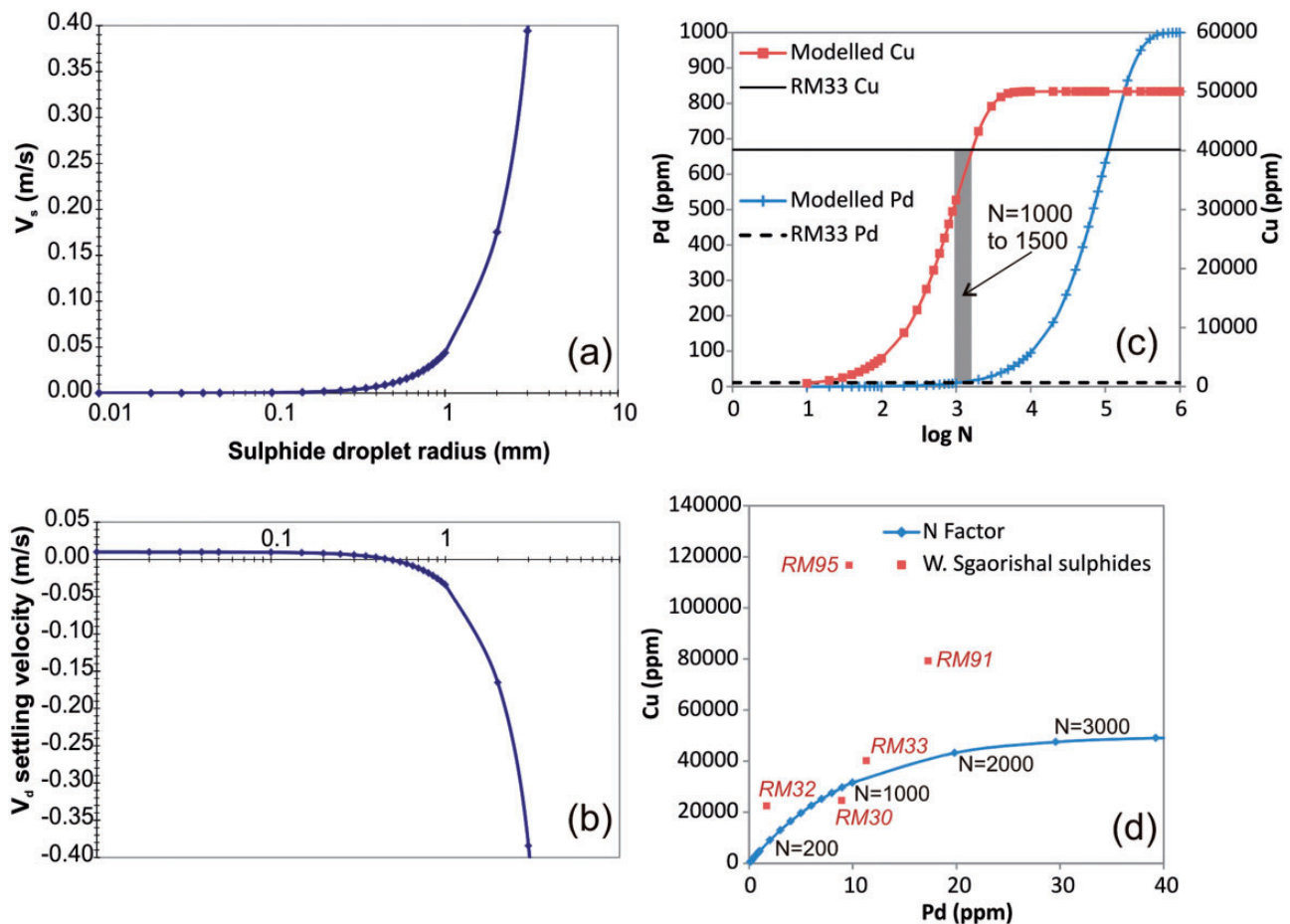
Fig. 8. Dynamic conduit modelling using the Hadamard–Rybczynski equation for sulphide settling: (a) sulphide velocity (V_s) vs size of a sulphide droplets (radius in mm); (b) sulphide settling velocity through a conduit (V_d) vs sulphide droplet radius. Sulphides will sink if $V_d < 0$. (c, d) *N*-factor modelling: (c) *N*-factor (plotted as log *N*) vs Pd and Cu concentration in the sulphide liquid. Continuous horizontal line delineates the Cu concentration in the sulphide liquid from the margin of plug 1 (RM33); the dashed horizontal line is for Pd. Both Cu and Pd were calculated from the bulk-rock geochemistry normalized to 100% sulphide [using the method outlined by Huminicki *et al.* (2005)]. Shaded rectangle shows the range of modelled log *N* values that fit Cu and Pd. (d) Modelled Cu and Pd concentrations in sulphides according to various values of *N* (labelled). Plotted for comparison are the calculated mean Cu abundances of the sulphide liquid [calculated by normalizing the bulk Cu concentration to 100% sulphide, using the method outlined by Huminicki *et al.* (2005)] and weighted mean Pd abundances (per sample weighted according to the number of analyses of chalcopyrite, pentlandite and pyrrhotite) for sulphides from plug 1, centre and margins.

observe two sets of olivine phenocrysts in the M9 dyke, thus highlighting that the bulk composition of this dyke is not suitable for use in modelling the parental magma.

According to the equation of Li & Ripley (2005), pressure (i.e. depth) has little effect on SCSS in comparison with temperature. Therefore if we reduce the ambient temperature to 1200°C (i.e. still 100°C above the liquidus temperature of sulphide) we see a significant drop in SCSS, to ~1600 ppm for the ultramafic plugs and ~1000 ppm for the gabbroic plugs. Accommodating for the bulk geochemical analyses incorporating up to 50% cumulus olivine for the ultramafic plugs, and using this lower temperature, we suggest that SCSS is within the range of the S content now observed in plugs across Rum. Coupled with observations of sulphide mineral embayments in cumulus olivine (as noted above), and Li & Ripley's calculations of decreasing SCSS with fractional crystallization of a

magma, it is plausible to assume that sulphide saturation could be achieved deeper in the magmatic system of Rum, prior to plug emplacement.

Several examples of sulphide liquid entrainment in magma conduits have been recorded worldwide; for example, the Norilsk–Talnakh magma conduit setting for orthomagmatic Ni–Cu–PGE mineralization, in which sulphides were initially exsolved in a deeper staging chamber before being flushed out to higher magmatic plumbing system levels (Brügmann *et al.*, 1993; Lightfoot & Keays, 2005). Sulphide entrainment is also suggested for the Platreef (Bushveld Complex) where sulphides were transported away from a deeper zone of sulphide liquid formation (McDonald & Holwell, 2007; McDonald *et al.*, 2009; Ihlenfeld & Keays, 2011; Sharman *et al.*, 2013). In the Platreef, evidence for this sulphide transportation was based on Cu/Pd, S/Se ratios, S-isotope compositions and trapped sulphide

melt inclusions (Holwell *et al.*, 2011). Clearly, the process of entrainment of pre-formed sulphides, other silicate minerals and xenoliths is a common feature of many magmatic systems. However, in many of these cases only one part of the full system is exposed, with earlier processes at depth being inferred. The volcanic plugs and the Layered Suite of Rum provide a rare opportunity to compare layered intrusion and volcanic pipe compositions and mechanisms of sulphide transport at the same present-day erosional level.

The $\delta^{34}S$ composition of the peridotite plugs ($+0.1 \pm 1.0‰$, excluding plugs 1 and 2) and peridotite cyclic units of the ELS ($–0.5 \pm 1.4‰$; Supplementary Material Table E) overlap with the typical Icelandic mantle plume range of $–2.0‰$ to $+0.4‰$ (Torssander, 1989), mid-ocean ridge basalt (MORB) $–0.91 \pm 0.5‰$ (Labidi *et al.*, 2012) and the picritic Trotternish Sills on the Isle of Skye with average $\delta^{34}S$ of $–2.3 \pm 1.5‰$ (Hughes *et al.*, 2015). Thus we suggest that, for most plugs and the ELS, S-saturation was reached prior to emplacement, in the deeper magmatic plumbing system where olivine crystallization and fractionation was taking place, and did not involve the addition of crustal sulphur with $\delta^{34}S$ different from magmatic compositions. We note that the $\delta^{34}S$ values observed in the ELS and plugs (excluding plugs 1 and 2), are slightly heavier ($–0.5$ to $+0.1 \pm 1‰$) than the Icelandic plume $\delta^{34}S$ signature of $–0.8‰$ to $–2.3‰$ [Torssander (1989) and Hughes *et al.* (2015), respectively] and that this may be due to small changes in the magmatic source signature. With ejection of crystal mushes from a staging chamber, sulphide liquid was entrained and emplaced into the peridotite plug magma conduits and Rum Layered Suite alike. However, in the case of plugs 1 and 2 significant deviation of $\delta^{34}S$ and elevation of S/Se ratio indicates that localized crustal contamination also took place.

Potential crustal S-sources for the West and Loch Sgaorishal plugs (plugs 1 and 2)

The $\delta^{34}S$ of plug 1 (West Sgaorishal) ranges from $–14.7$ to $–8.0‰$ with a S/Se ratio of sulphide minerals ranging from 3000 to 12 000, whereas the $\delta^{34}S$ of plug 2 (Loch Sgaorishal) varies from $–6.5$ to $–2.9‰$ (Fig. 7a). Further, the sulphide S/Se ratios of plug 1 are elevated above the range of most ELS sulphides, and often exceed 10 000 (a critical value for crustal sedimentary sulphide compositions; Ihlenfeld & Keays, 2011, and references therein). These S-isotope compositions are significantly lighter than typical mantle or Icelandic plume values, and, together with S/Se, demonstrate that crustal S must have been added to the plug 1 and 2 magmas. There is also a change in textural character of the sulphides in plug 1, which became more abundant and coarser grained. Hence the following questions arise: what was this sulphur source, and why is this light $\delta^{34}S$ recorded only in two plugs from NW Rum?

The $\delta^{34}S$ of sedimentary S (typically pyrite) can be highly variable owing to bacterially mediated sulphate reduction processes during diagenesis. The range of $\delta^{34}S$ can be of the order of tens of per mil (‰) with both negative and positive values. Palaeozoic and Mesozoic sedimentary sulphides generally have more negative values than those observed in Precambrian rocks (Canfield & Teske, 1996; Parnell *et al.*, 2010).

Most plugs on Rum have intruded through Torridonian (Applecross Formation) sandstones at the current erosion level, but the NW tip of plug 1 also intrudes the unconformable base of a sequence of Triassic limestones and calcretes (Binns *et al.*, 1974; Fyfe *et al.*, 1993). Hughes *et al.* (2015) established that the $\delta^{34}S$ of these Triassic sediments is isotopically heavy (with very low S concentrations) and thus cannot account for the $\delta^{34}S$ of plugs 1 and 2 via assimilation. This leaves three possible explanations: (1) Torridonian lacustrine sediments with a light $\delta^{34}S$ (e.g. Parnell *et al.*, 2010) are present below plugs 1 and 2; (2) a segment of Jurassic mudrock with suitably light $\delta^{34}S$ occurs in a downthrown faulted block of a major fault zone (e.g. Main Ring Fault) through which plugs 1 and 2 have intruded; or (3) the $\delta^{34}S$ signature of plugs 1 and 2 is derived from above the current erosion level and involves the Lower Jurassic Broadford Group that probably covered this area at the time of conduit activity.

Despite some Torridonian lacustrine sediments from the mainland Stoer Group having $\delta^{34}S$ as low as $–30.1 \pm 17.3‰$ (Parnell *et al.*, 2010), all the Sleat and Torridon Group Mesoproterozoic sediments analysed by Hughes *et al.* (2015) had values $> 0.0‰$. Further, the Stoer Group is not recorded in the sedimentary pile exposed on either Skye or Rum, suggesting that scenario (1) is extremely unlikely.

Hebridean Jurassic mudrock and ironstone $\delta^{34}S$ values range from $–10$ to $–35‰$, and associated basaltic dykes intruded through this sequence record $\delta^{34}S$ values as light as $–30.7‰$ (Hughes *et al.*, 2015). Blocks of Jurassic mudrock are recorded as being present within the Main Ring Fault on Rum at Allt nam Bà and near Dibidil (Emeleus & Troll, 2008; Figs 1 and 2c). In contrast, no such sedimentary blocks are reported from the Long Loch Fault, not least owing to this being a strike-slip fault with no vertical motion that would have downthrown these sedimentary units. It is possible, however, that the subsurface route of the plug magma conduits could have intersected a downthrown block of Jurassic mudrocks, assuming that these conduits were fed from somewhere near the centre of the Rum volcanic edifice. However, only plugs 1 and 2 from the NW quadrant of the island record this light $\delta^{34}S$ and the absence of such a light $\delta^{34}S$ in plugs 3–5 renders this scenario highly improbable; and necessarily very localized, if true.

By a process of elimination, to account for the light $\delta^{34}S$, we are left with a scenario whereby crustal sulphur contamination demonstrably took place only in plugs 1 and 2. If contamination were taking place above the current erosion level, in Lower Jurassic sediments

that very probably overlay this region, there remains a problem as to how these crustally contaminated sulphides are now present below the level of the potential contaminant. One possibility may be that the sulphides moved down the plug or conduit. Below we consider whether this is feasible given the upward injection of magma in a conduit, and whether the observed characteristics of the sulphides in plugs 1 and 2 support this model. What were the physical constraints on sulphides sinking and could this effect have been so localized that the other plugs (3–5) further 'downhill' on the NW quadrant of Rum, be too low in altitude to record this process?

Dynamic conduit modelling and sulphide sinking
Hadamard–Rybczynski conduit modelling
The settling of sulphide liquid droplets through a magma conduit can be modelled either by using Stoke's Law or by the Hadamard–Rybczynski equation (e.g. Lightfoot *et al.*, 1984) as established by the experiments of de Bremond d'Ars *et al.* (2001). The latter takes into account the non-Newtonian fluid properties in the conduit, as well as the differences in both density and viscosity of the silicate and sulphide liquids present in the system, and is expressed as

$$V_s = \frac{1}{3} \left[\frac{\Delta\rho g r^2}{\mu f} \right] \frac{[\mu f + \mu d]}{[\mu f + \frac{3}{2}\mu d]} \qquad (1)$$

where V_s is settling velocity (m s^{-1}), r is sulphide droplet radius (m), $\Delta\rho$ is the difference in density between sulphide liquid and silicate magma ($= 1400$ kg m^{-3}), μf and μd are the viscosities of silicate magma (0·1 Pa s; Paterson *et al.*, 1998) and sulphide liquid (0·01 Pa s) respectively, and g is the acceleration due to gravity (9·8 m s^{-2}). Sulphide droplets will sink (with velocity V_d) through the conduit pipe once the settling velocity (V_s) exceeds the upward velocity of magma intruding into and through the pipe (V_z), such that

$$V_d = V_z - V_s. \qquad (2)$$

Sulphide droplet settling occurs when $V_d < 0$ m s^{-1}. The analogue experiments of de Bremond d'Ars *et al.* (2001) indicated that sulphide droplets can be transported in suspension by flowing magmas, and that owing to the large surface tension of the droplets, they do not coalesce during active transport. In part, this could explain the disparity and size of sulphide minerals in peridotite plugs 4–12. These plugs generally do not record matrix banding or indentation layering, suggesting that prolonged quiescent periods were not prevalent during cooling, hence perturbing the ability of the conduit to form crystal layering (e.g. Wadsworth, 1994) and thus arresting sulphide droplet settling and coalescence. Further, the low abundance of sulphides in plugs 4–12 would also hamper coalescence. The size and distribution of fine sulphides in these plugs probably reflects the mode of transportation and entrainment that occurred during conduit activity.

For scenarios involving higher volumes of sulphide liquid, plots of V_s and V_d according to sulphide droplet radius are presented in Fig. 8a and b. Sulphides in the margins of plug 1 range in diameter from 0·5 to 4 mm (Table 2); most intercumulus sulphides are 1–3 mm in diameter. V_z was varied in equation (2) until sulphides of the minimum average radius observed in the margin of plug 1 ($r \sim 0.5$ mm) had $V_d < 0$ m s^{-1}. This required an upward magma velocity of 0·01 m s^{-1} (Fig. 8a and b), such that sulphide droplets would sink through the conduit at a rate of 0·001 m s^{-1} (V_d). By lowering V_z further to 0·001 m s^{-1}, sulphides with $r = 0.2$ mm would also begin to sink at a similar rate. Thus, the upward flow of magma through the conduit would essentially have to have ceased before sulphide droplets of the sizes observed in the margins of plug 1 would settle. The viscosity of the silicate magma was assumed to be 0·1 Pa s (Paterson *et al.*, 1998); however, if the conduit was instead filled with olivine phenocrysts entrained in basaltic magma then the overall effective viscosity of the 'silicate magma' would be higher. Holness *et al.* (2012) suggested a crystal load in the range of 10–40 vol. % for the peridotite plugs, based on the volume of phenocrysts entrained in picrite dykes on Rum. Even by increasing viscosity to 1 Pa s [i.e. an assumed 50% crystal mush entrained in a mafic magma, with viscosity $= 1$ Pa s based on Paterson *et al.* (1998)] at $V_z = 0.001$ m s^{-1}, sulphides of $r \sim 0.5$ mm would still be capable of sinking through the conduit. In summary, it is possible that sulphide liquids forming through crustal contamination above the present-day level of erosion and exposure of plug 1 (and plug 2) would have sunk through the conduit once active upwards magma injection had ceased. Sulphide liquid sinking may have taken place either in a passively cooling (stationary) environment and/or sulphide liquid was 'sucked' downwards if magma withdrawal were taking place.

By assuming that the cooling rate of a stationary magma is controlled by Newton's Law of Cooling,

$$T = T_a + (T_o - T_a)e^{-\kappa t} \qquad (3)$$

it would take the margin of plug 1 *c.* 5 days to cool below 1100°C, where T_a is the temperature of the country rock [assumed to be 600°C, based on Holness *et al.* (2012)], T_o is the initial magma temperature of the conduit [assumed to be 1400°C; Holness *et al.* (2012)], T is the target temperature of 1100°C for the sulphide liquidus (e.g. Bowles *et al.*, 2011) and κ is a thermal diffusivity constant of 10^{-6} m^2 s^{-1}. Given a downward velocity V_d of 0·001 m s^{-1} for sulphide droplets through the quiescent conduit, sulphides would be capable of settling through a distance of the order of 400 m, downwards from the initial level of S-saturation. As mentioned above, however, constraints on the SCSS of these plugs may suggest that their emplacement temperature was lower than 1400°C. Therefore if we use 1200°C as the emplacement temperature, we estimate

that sulphides could still have settled more than 100 m down the conduit.

Ultimately, this settling distance is likely to be subject to estimation errors; for example, as sulphide droplets coalesce during settling, their settling velocity will change. In addition, as the conduit cools towards 1100°C, the effective viscosity of both the sulphide liquid and silicate magma will increase, thus slowing its descent. The 'permeability' of the host silicate mush (i.e. amount of partial melt and degree of ponding of sulphide liquid above areas of low permeability; e.g. Holwell & McDonald, 2006; Hutchinson & McDonald, 2008) may not be uniform throughout a single volcanic plug. However, the interfacial tension at silicate–sulphide liquid interfaces may preclude sinking of sulphide droplets below a critical size range (e.g. Mungall & Su, 2005). This depends on the proportions of silicate melt to solidified silicate minerals in the system, and would suggest that compaction-driven sulphide segregation is possible (Rose & Brenan, 2001).

The estimated thickness of Triassic sediments in the Hebrides Basin in the vicinity of Rum on the 'Skye High' of this Mesozoic sedimentary basin ranges from tens of metres on Ardnamurchan, to 100 m at Raasay off the Isle of Skye, and 300 m at Gruinard Bay on the Scottish mainland (Steel *et al.*, 1975). Given that the current erosion level of plug 1 occurs at the base of these Triassic sediments (Figs 2a and 9a) and the estimated minimum potential settling distance of sulphide droplets is 100 m (assuming a lower emplacement temperature of 1200°C) to 400 m [using the Holness *et al.* (2012) emplacement temperature of 1400°C], this is within reach of S-rich lower Jurassic sediment horizon(s), assumed to have been present above the current erosion level (Fig. 9a). Assimilation of wall-rock sediments, particularly light δ^{34}S crustal sulphur from Jurassic units, would induce sulphide saturation at a high level in the conduit (above the current erosion level; e.g. Fig. 9b). Thus, we can reasonably envisage that once active magma-mush injection had ceased, silicate and sulphide liquids from above sank through the conduit, forming olivine cumulates with interstitial sulphide liquid that recorded light crustal S isotope compositions and high S/Se ratios inherited from hundreds of metres above (e.g. Fig. 9c).

Although plug 2 also records δ^{34}S in sulphides significantly less than the local magmatic compositions of around 0‰, it has lower abundances of sulphide than plug 1. Projecting the dip of the base of the Triassic sedimentary units near plug 1 (approximately 20° NW; Fig. 9a) and even accounting for the current topography and elevation of the area between plugs 1 and 2, the lower sulphide abundance in plug 2 may reflect the greater distance between the potential Lower Jurassic contamination zone and the present-day level of exposure (Fig. 9a). Further, the lack of a crustal δ^{34}S signature in plugs 3, 4 and 5 is consistent with the model, in that their current level of exposure is >400 m below the projected contamination horizon, so that any sulphides that

did settle downwards are likely to have been removed by erosion (i.e. Fig. 9a). The lack of a crustal δ^{34}S signature in plugs from elsewhere on the island, particularly farther east, may also suggest that the Mesozoic sedimentary sequence of the Hebrides Basin was not present, as the Isle of Rum sits on the 'Skye High' within the basin such that only the feather-edge of the basin's sediments could have been deposited over part of the island (see Hughes *et al.*, 2015).

Jurassic shale geochemical interaction with volcanic plugs

The sedimentary host rocks to the volcanic plugs (Triassic, Fig. 2a; Torridonian, Fig. 2a–c) typically appear bleached, fissile and metasomatized. Detailed studies of *in situ* anatexis of these rocks have provided insights into the longevity of the plugs as active magma conduits (e.g. Holness, 1999; Holness *et al.*, 2012). Static melting occurred up to 15 m from the gabbro plugs and 6 m from the larger peridotite plugs, suggesting that the peridotite plugs were a relatively short-lived magma conduits (active for *c.* 1–2 years; Holness *et al.*, 2012) whereas the gabbro plugs were longer lived features (*c.* 40 years; Holness, 1999). However, Holness (1999) concluded that anatectic melt migration did not occur, so that very limited contamination of the plug margins was likely to have taken place. However, Yallup *et al.* (2013) and Hughes *et al.* (2015) (and references therein) demonstrated that the volatile content (S, C, H_2O, etc.) of mudrocks is particularly vulnerable to mobilization by magmas during contact metamorphism of wall-rocks and/or their brecciation. In this way, we envisage a scenario whereby S is preferentially mobilized, imparting a strong crustal contamination signature onto the plug magmas, but without other non-volatile trace element contamination.

Comparison with Paleogene macrodykes in East Greenland and other similar intrusions

A similar set of geological circumstances exists in East Greenland, where Holwell *et al.* (2012) described a suite of mineralized macrodykes, radiating away from the Skaergaard intrusion and intruding Archaean basement and overlying pyrite-rich Cretaceous black shales (with δ^{34}S –23 to –30‰) and Paleogene flood basalts. Magmatic Cu–PGE–Au sulphide mineralization, with crustal δ^{34}S signatures (–10 to –26‰), is present along the margins of the subvertical Miki Fjord Macrodyke, which is observed to intrude all three lithological units. Further north, the Togeda Macrodyke, which is exposed at a level where it intrudes the basement gneiss, has similar sulphides that have a light S-isotope signature (Holwell *et al.*, 2012). Holwell *et al.* (2012) concluded in both cases that Cretaceous shales were the trigger for sulphide saturation and that sulphide droplets were entrained within the macrodyke magmas during intrusion. The presence of sulphides in the Togeda Macrodyke, beneath the stratigraphic level of the contaminant, was
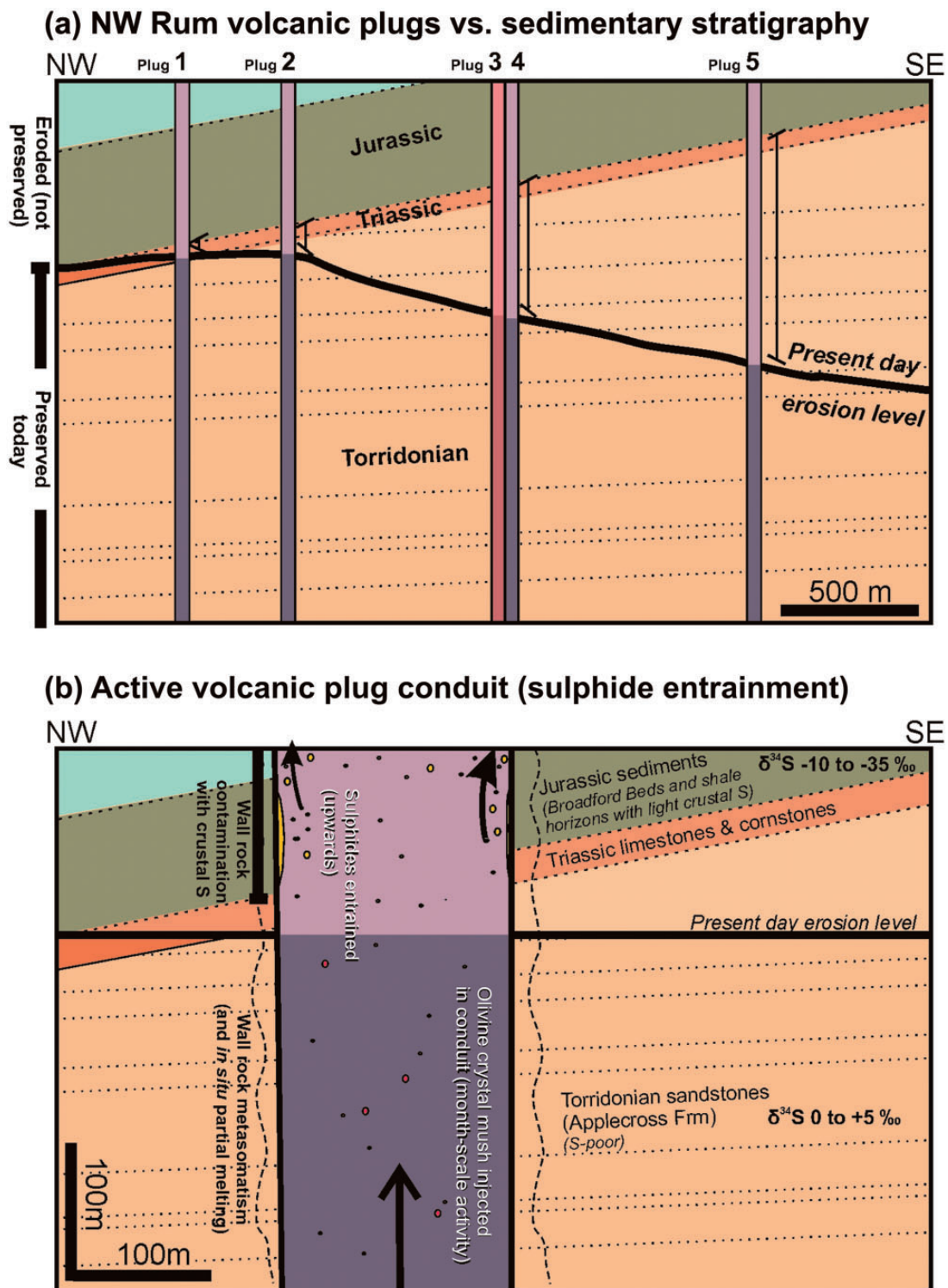
Fig. 9. Schematic cross-sections of the crustal sulphur contamination scenario for NW Rum. (a) Schematic cross-section of NW Rum showing plugs 1–5 in the vicinity of Sgaorishal. Owing to the orientation of the Mesozoic Hebridean Basin Triassic and Jurassic sediments relative to the present-day topography, the current exposures of plugs 3, 4 and 5 are too great a distance below the Jurassic contamination horizon to record crustal δ^{34}S and voluminous sulphide liquids. However, plugs 1 and 2 still record light crustal δ^{34}S. (b) Active volcanic plug intrudes through Torridonian sediments, and Triassic and Jurassic sediments of the Hebrides Basin (since eroded) above. The plug entrains tiny droplets of high-tenor sulphide liquid from a staging chamber. Wall-rock metasomatism and partial melting (especially recorded in the siliceous Torridonian Applecross Formation sandstones) takes place. In the upper portions of the plug, S-rich shales and siltstones from the Jurassic sediments contaminate the magmas with isotopically light crustal S. (c) Active magma intrusion of volcanic plug ceases, and magma-entrained olivine mushes are left to settle through the conduit (forming cumulate layers, particularly at the conduit margins). Sulphide droplets entrained in the plug, including more voluminous sulphide liquids from crustal S contamination horizons (above) in Jurassic sedimentary units, settle through the conduit. Sulphide liquids amalgamate during settling, and form an interstitial or intercumulus phase around the cumulate olivine. Sulphide liquid is particularly abundant around the conduit margins (owing to wall-rock S contamination) and has a higher concentration of PGE, higher S/Se ratio and lighter δ^{34}S.
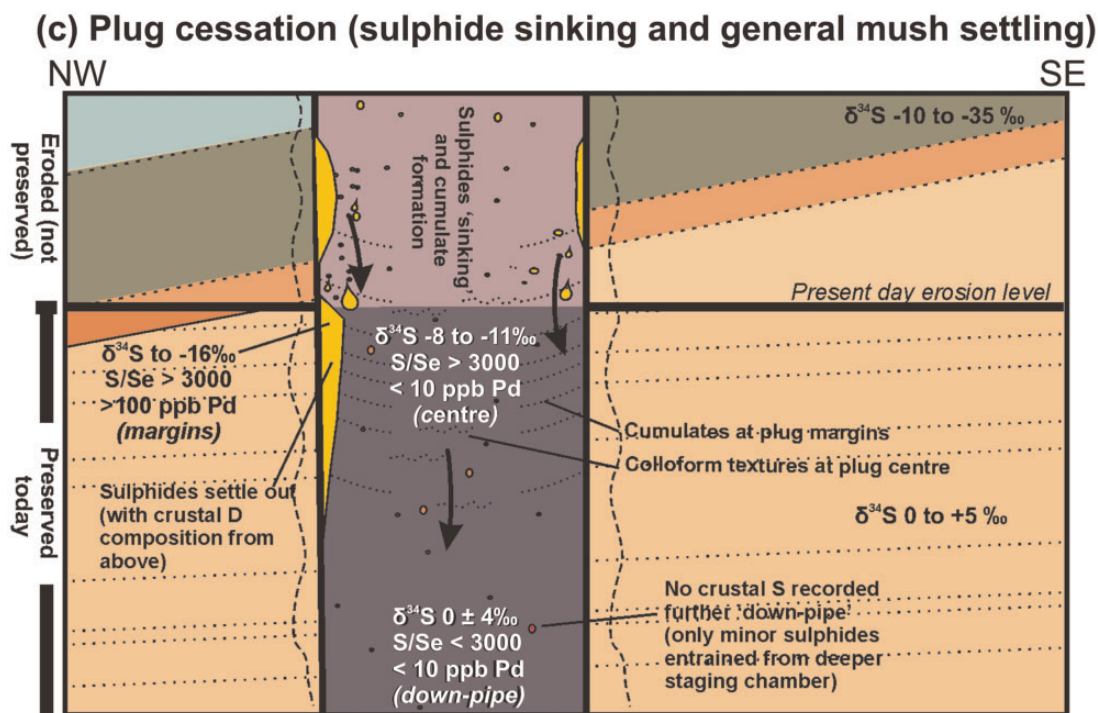
Fig. 9. Continued

explained by northward injection of magma, which could then incorporate S from sediments exposed deeper to the south (Holwell *et al.*, 2012).

A similar situation to that described above for the Rum plugs is also possible for the Togeda Macrodyke. The Cretaceous sedimentary units are inferred to have been present some 500 m or so above the present erosion level. Given the much larger size of the droplets (up to 10 mm) in the macrodykes compared with the Rum plugs (mostly 1–3 mm), the likelihood of large droplets settling down through the dyke conduit by a vertical distance of up to 500 m is plausible. For example, assuming a sulphide droplet with radius (r) of 0·5 mm and a silicate liquid (not crystal mush) of viscosity 0·1 Pa s, then owing to the silicate–sulphide liquid density difference, the sulphide droplets would be capable of sinking through a magma conduit with upward silicate magma velocities (V_z) of up to 1·1 m s^{-1}. However, in a dyke scenario, lateral movement of magmas along the dyke (owing to a pressure gradient from the point of intrusion along an opening fracture) must also be factored in. Hence both lateral and downward migration of sulphide droplets may be envisaged for planar features such as dykes (e.g. Todega Macrodyke), in contrast to pipe-shaped conduits.

The downward movement of sulphide liquids in a cooling magmatic system has also been suggested for ultramafic complexes in Madagascar (McDonald, 2008). In this model, sulphide liquids migrate laterally, as well as downwards, towards the centre of the intrusion during crystallization. During their migration, the sulphide liquids fractionated such that Pt- and Pd-bearing PGM

exsolved from, and detached from, the sulphide liquid (becoming trapped in olivine mushes), leaving Cu-rich sulphide liquid to continue sinking towards the centre of the intrusion (McDonald, 2008).

Our model of sulphide sinking in a cooling magmatic system (where magma flow has recently ceased) differs markedly from sulphide sinking models suggested for other mineralized conduit settings; for example, at Norilsk–Talnakh where Arndt (2011) envisaged that sulphide liquids sank (or were re-injected) through an active silicate magma conduit, with a significant upward velocity of magma injected from beneath. Sulphide pools may be re-entrained by pulses or batches of new magma (e.g. Robertson *et al.*, 2014), leading to complex scenarios of re-deposition within large, dynamic or long-lived conduit systems, with ultimate sulphide tenor upgrading (Barnes *et al.*, 2016, and references therein).

N-*factor modelling: silicate/sulphide liquid ratios*
Another parameter that can be calculated for a sulphide-bearing conduit is the proportion of sulphide liquid to silicate magma within the system. In a closed system, this is typically denoted by the 'R-factor'; however, in the case of open-system conduits this is termed the 'N-factor' and was modelled for the sill-hosted Norilsk–Talnakh Ni–Cu–PGE orthomagmatic mineralization in Siberia (Brügmann *et al.*, 1993; Naldrett & Fedorenko, 1995; Naldrett *et al.*, 1996). In an open system such as a magma conduit silicate magma batches are flushed through the conduit system. If this system is

S-saturated, sulphide liquids may become trapped within the conduit whilst silicate magmas continue to flush through. Owing to their strong chalcophile nature, PGE and Cu will partition from each fresh silicate magma batch into the resident sulphide liquid, thereby upgrading the PGE tenor of this sulphide in a mechanism analogous to zone refining (Brügmann *et al.*, 1993; Naldrett & Fedorenko, 1995; Naldrett *et al.*, 1996). The proportion of silicate magma (as a time integrated volume) relative to the volume of the sulphide liquid will determine this degree of PGE upgrading.

The *N*-factor is typically used for conduits in which magmas move upwards past sulphide accumulations. However, in the situation we propose for Rum, sulphide droplets are formed at the top of the magma conduit and slowly settle through it (e.g. Brügmann *et al.*, 1993). The effect is the same; in both cases silicate magma and sulphide liquids must migrate past one another to achieve upgrading of PGE tenor. Thus the *N*-factor model is appropriate in this instance to assess the volumes of ambient sulphide liquid in the conduit.

The *N*-factor equation, based on Cox *et al.* (1979) is as follows:

$$Y_i = X_i\{D - [(D-1)\mathrm{e}^{-(1/D)N}]\} \tag{4}$$

where Y_i is the concentration of metal i in the sulphide, X_i is the initial concentration of metal i in the silicate, and D is the partition coefficient for metal i between silicate and sulphide;

$$N = \frac{\text{volume silicate magma}}{\text{volume sulphide liquid}}. \tag{5}$$

As the value of N increases, the concentration of strongly chalcophile metals such as Pt and Pd rapidly increases. For plug 1, the concentration of trace elements such as Pd and Cu according to the volume ratio of silicate magma to sulphide liquid (*N*-factor) can be modelled using equation (4), assuming $D_{Cu} = 1470$ and $D_{Pd} = 190\,000$ (Mungall & Brenan, 2014), with an initial silicate magma composition of 50 ppm Cu and 10 ppb Pd (comparable with picritic compositions and Cu and Pd abundances in other low-sulphide plugs such as plug 12). By finding the intersection between the model curves for Pd and Cu and the measured concentration of these metals in the plug, we can estimate that the ratio of silicate magma to sulphide liquid (*N*-factor) ranged from 1000 to 1500 (specifically using sample RM33 from plug 1) (Fig. 8c).

To cross-check if the *N*-factor calculated is reasonable, we have used the average abundance of Pd measured in sulphides (Table 3) calculated per sample for plug 1, and plotted this against the calculated Cu abundance for a homogenized sulphide liquid, based on assigning all bulk-rock Cu to chalcopyrite, and normalizing to 100% sulphides. As sulphide assemblages comprise pyrrhotite, pentlandite and chalcopyrite (with only accessory bornite, chalcocite and galena), we have followed the method of Huminicki *et al.* (2005) using the whole-rock measured abundances of S, Cu, Ni and Fe. All of the whole-rock Cu budget was assigned to chalcopyrite, and after subtracting the mass of S required, and the mass of Ni bound within olivine [assuming a Ni content of 2400 ppm in olivine and an average of 60% olivine in the plug, based on Holness *et al.* (2012)] all of the remaining Ni was assigned to pentlandite. The proportion of pyrrhotite was then estimated from the remaining S. Following the observations and methods of Holwell & McDonald (2007), such that chalcopyrite contains negligible PGE in solid solution, we then recalculate the measured whole-rock PGE content to 100% pyrrhotite + pentlandite, as these are the principal PGE-bearing base metal sulphides. By this method, the Cu and Pd compositions of sulphides in plug 1 can be modelled by equation (4) if $N = 1000$–1500 (Fig. 8c and d). This includes the centre of the plug (e.g. RM30). However, the outlier RM95 at the southern plug margin has a substantially higher concentration of Cu (almost 120 000 ppm), which may suggest that the margin of the plug (as represented by RM95) has acquired extra Cu from the surrounding wall-rock. The Triassic Sandstone Formation in this area contains rare malachite reported with carbonate calcretions (Emeleus & Troll, 2008).

The significance of sulphide sinking versus upward entrainment

Comparison with examples outside the BPIP shows that a process of sulphide sinking through cooling, recently inactive conduits may well be widespread and could account for the presence of high-volume sulphides with crustal S compositions at levels stratigraphically lower than that at which they originally formed. Thus, the study of mineralized magmatic sulphide systems also needs to consider the possibility of contamination from sources above the level of mineralization, which may no longer be exposed. In terms of exploration models, this is significant in that intrusions exposed below the stratigraphic level of any potential contaminant (or where possible contaminants have been eroded) still have the potential to host magmatic sulphides. If a settling sulphide liquid had the ability to pond in a depression in the magmatic plumbing system, then massive sulphide accumulations that result from crustal contamination could potentially be found hundreds of metres below the level of the contaminant that triggered sulphide saturation. Our work provides quantifiable and traceable evidence for the processes of sulphide sinking. As such, it offers support to the growing number of studies that cite sulphide sinking, slumping and/or re-injection within conduits as a mechanism for magmatic sulphide accumulation and upgrading (Benko *et al.*, 2015; Saumur *et al.*, 2015; Barnes *et al.*, 2016, and references therein; Saumur & Cruden, 2016). This contrasts with the more traditional view of upward entrainment of sulphides into higher level intrusions (e.g. Holwell & McDonald, 2007; Naldrett *et al.*, 2009, 2011).

CONCLUSIONS

1. The peridotite plugs on the Isle of Rum were intruded as olivine-rich crystal mushes suspended in a basaltic or picritic magma that also entrained sulphide liquid.
2. Based on the elevation and corresponding compositions of the plugs and cyclic units, it is unlikely that the Rum Layered Suite directly fed all these volcanic conduits. Instead we suggest that a separate, deeper, staging chamber was responsible for the periodic and discrete intrusion of peridotitic crystal mushes with entrained sulphide into both the Rum Layered Suite and the volcanic conduits represented by the plugs.
3. Most plugs have a magmatic whole-rock δ^{34}S signature of $+0\cdot1 \pm 1\cdot0\text{‰}$, which overlaps with the whole-rock δ^{34}S signature of the ELS ($-0\cdot5 \pm 1\cdot4\text{‰}$) and proto-Icelandic plume values recorded elsewhere in the NAIP ($-2\cdot3 \pm 1\cdot5\text{‰}$; Hughes *et al.*, 2015). In addition, whole-rock and sulphide-specific PGE abundances in plugs lacking crustal contamination signatures overlap compositions in the ELS.
4. Two plugs in the NW of the island have a distinctive crustal δ^{34}S signature (ranging from $-14\cdot7$ to $+0\cdot3\text{‰}$) and elevated S/Se ratios (up to 12 130), unlike any of the other plugs on Rum. Projecting the Hebrides Basin sediment stratigraphy above the preserved unconformable base of Triassic rocks (Fig. 9a), the volcanic conduits would probably have been emplaced through a thick package of Jurassic mudrocks with characteristically light δ^{34}S ($-33\cdot8$ to $-14\cdot7\text{‰}$), forcing sulphide supersaturation and the formation of voluminous immiscible sulphide liquid, locally and at a near-surface level (Fig. 9b).
5. Once active magma transport had ceased, the sulphide liquids would sink back through the conduit. Based on modelling of the conduit mush viscosity and cooling rates, this settling would take place over a distance of up to 400 m and over a period of a few days, resulting in the poikilitic and net-textures preserved today. Sulphides previously entrained in the crystal mush from the staging chamber, and this secondary immiscible sulphide liquid, became amalgamated upon sulphide supersaturation. Thus the δ^{34}S of these plugs (1 and 2) is a mixture of both early and later sulphide liquids, although the crustal isotopic contamination signature dominates owing to the production of greater volumes of sulphide.
6. Given the current topography in the NW of Rum, the other plugs probably record deeper level sulphides in the plug conduit plumbing system (i.e. with uncontaminated magmatic δ^{34}S), and any crustal S influence (if originally present) has since been removed by erosion.
7. *N*-factor modelling for the crustally contaminated plugs (1 and 2) suggests a silicate magma to sulphide liquid ratio of 1000–1500.
8. We suggest that this sulphide sinking process (within a cooling non-active conduit or during magma 'suck-back') may be observed in other vertical or inclined magma conduits globally; for example, in the macrodykes of East Greenland. This model may be used to explain S-isotopic and S/Se ratios that are indicative of contamination of magmas by crustal S although no suitable lithology is present either in the immediate host rocks or deeper in the system.

SUPPLEMENTARY DATA

Supplementary data for this paper are available at *Journal of Petrology* online.

REFERENCES

Andersen, J. C. Ø., Rasmussen, H., Nielsen, T. F. D. & Rønsbo, J. G. (1998). The Triple Group and the Platinova gold and palladium reefs in the Skaergaard Intrusion: Stratigraphic and petrographic relations. *Economic Geology* **93**, 488–509.

Andersen, J. C. Ø., Power, M. R. & Momme, P. (2002). Platinum-group elements in the Palaeogene North Atlantic Igneous Province. In: Cabri, L. J. (ed.) *The geology, geochemistry, mineralogy and mineral beneficiation of platinum-group elements. Canadian Institute of Mining, Metallurgy and Petroleum (CIM) Special Volume* **54**, 637–668.

Arndt, N. T. (2011). Insights into the geologic setting and origin of Ni–Cu–PGE sulfide deposits of the Norilsk–Talnakh region, Siberia. *Reviews in Economic Geology* **17**, 190–215.

Arnold, R. G. (1971). Evidence for liquid immiscibility in the system FeS–S. *Economic Geology* **66**, 1121–1130.

Barnes, S. J., Fiorentini, M. L., Austin, P., Gessner, K., Hough, R. M. & Squelch, A. P. (2008). Three-dimensional morphology of magmatic sulfides sheds light on ore formation and sulfide melt migration. *Geology* **36**, 655–658.

Barnes, S. J., Cruden, A. R., Arndt, N. & Saumur, B. M. (2016). The mineral system approach applied to magmatic Ni–Cu–PGE sulphide deposits. *Ore Geology Reviews* (online first, in press).

Bédard, J. H., Sparks, R. S. J., Renner, R., Cheadle, M. J. & Hallworth, M.A. (1988). Peridotite sills and metasomatic gabbros in the Eastern Layered Series of the Rhum complex. *Journal of the Geological Society, London* **145**, 207–224.

Benko, Z., Mogessie, A., Molnar, F., Severson, M. J., Hauck, S. A. & Raic, S. (2015). Partial melting processes and Cu–Ni–PGE mineralization in the footwall of the South Kawishiwi Intrusion at the Spruce Road deposit, Duluth Complex, Minnesota, USA. *Economic Geology* **110**, 1269–1293.

Binns, P. E., McQuillin, R. & Kenolty, K. (1974). *The geology of the Sea of the Hebrides. Report of the Institute of Geological Sciences*, p. 1269–1293.

Bird, D. K., Brooks, D. K., Gannicott, R. A. & Turner, P. A. (1991). A gold-bearing horizon in the Skaergaard Intrusion, East Greenland. *Economic Geology* **86**, 1083–1092.

Bowles, J. F. W., Howie, R. A., Vaughan, D. J. & Zussman, J. (2011). *Rock-forming Minerals: Non-silicates; Oxides, Hydroxides and Sulphides*. Geological Society.

Brügmann, G. E., Naldrett, A. J., Asif, M., Lightfoot, P., Gorbachev, N. S. & Fedorenko, V. A. (1993). Siderophile and chalcophile metals as tracers of the evolution of the Siberian Trap in the Noril'sk region, Russia. *Geochimica et Cosmochimica Acta* **57**, 2001–2018.

Butcher, A. R., Young, I. M. & Faithfull, J. W. (1985). Finger structures in the Rhum Complex. *Geological Magazine* **122**, 491–502.

Butcher, A. R., Pirrie, D., Pritchard, H. M. & Fisher, P. (1999). Platinum-group mineralization in the Rum layered intrusion, Scottish Hebrides, UK. *Journal of the Geological Society, London* **156**, 213–216.

Cameron, E. M. (1994). Depletion of gold and LILE in the lower crust: Lewisian Complex, Scotland. *Journal of the Geological Society, London* **151**, 747–754.

Canfield, D., Raiswell, R., Westrich, J., Reaves, C. & Berner, R. (1986). The use of chromium reduction in the analysis of rediced inorganic sulphur in sediments and shales. *Chemical Geology*, **54**, 149–155.

Canfield, D. E. & Teske, A. (1996). Late Proterozoic rise in atmospheric oxygen concentration inferred from phylogenetic and sulphur-isotope studies. *Nature* **382**, 127–132.

Chambers, L. M., Pringle, M. S. & Parrish, R. R. (2005). Rapid formation of the Small Isles Tertiary centre constrained by precise $^{40}Ar/^{39}Ar$ and U–Pb ages. *Lithos* **79**, 367–384.

Chung, H.-Y. & Mungall, J. E. (2009). Physical constraints on the migration of immiscible fluids through partially molten silicates, with special reference to magmatic sulfide ores. *Earth and Planetary Science Letters* **286**, 14–22.

Cox, K. G., Bell, J. D. & Pankhurst, R. J. (1979). *The Interpretation of Igneous Rocks*. Allen & Unwin.

Czamanske, G. K., Kunilov, V. E., Zientek, M. L., Cabri, L. C., Likhachev, A. P., Calk, L. C. & Oscarson, R. I. (1992). A proton microprobe study of magmatic sulfide ores from the Norilsk–Talnakh District, Siberia. *Canadian Mineralogist* **30**, 249–287.

de Bremond d'Ars, J., Arndt, N. T. & Hallot, E. (2001). Analog experimental insights into the formation of magmatic sulphide deposits. *Earth and Planetary Science Letters* **186**, 371–381.

Emeleus, C. H. (1997). *Geology of Rum and the Adjacent Islands*. British Geological Survey.

Emeleus, C. H. & Bell, B. R. (2005). *British Regional Geology: The Palaeogene Volcanic Districts of Scotland*. British Geological Survey.

Emeleus, C. H. & Troll, V. R. (2008). *A geological excursion guide to Rum*. Edinburgh Geological Society.

Emeleus, C. H. & Troll, V. R. (2011). Recent research developments on the Isle of Rum, NW Scotland. *Geology Today* **27**, 184–193.

Faithfull, J. W. (1985). The lower Eastern Layered Series of Rhum. *Geological Magazine* **122**, 459–468.

Fyfe, J. A., Long, D. & Evans, D. (1993). *United Kingdom Offshore Regional Report: the Geology of the Malin–Hebrides Sea Area*. HMSO for the British Geological Survey.

Godel, B., Barnes, S.-J. & Maier, W. D. (2006). 3-D distribution of sulphide minerals in the Merensky Reef (Bushveld Complex, South Africa) and the J-M Reef (Stillwater Complex, USA) and their relationship to microstructures using X-ray computed tomography. *Journal of Petrology* **47**, 1853–1872.

Godel, B., Barnes, S. J. & Barnes, S.-J. (2013). Deposition mechanisms of magmatic sulphide liquids: Evidence from high-resolution X-ray computed tomography and trace element chemistry of komatiite-hosted disseminated sulphides. *Journal of Petrology* **54**, 1455–1481.

Hall, G. E. M., Pelchat, J. -C. & Loop, J. (1998). Separation and recovery of various sulphur species in sedimentary rocks for stable sulphur isotopic determination. *Chemical Geology,* **67**, 35–45.

Hamilton, M. A., Pearson, D. G., Thompson, R. N., Kelley, S. P. & Emeleus, C. H. (1998). Rapid eruption of Skye lavas inferred from precise U–Pb and Ar–Ar dating of the Rum and Cuillin plutonic complexes. *Nature* **394**, 260–263.

Hayes, B., Bédard, J. H., Hryciuk, M., Wing, B., Nabelek, P., McDonald, W. D. & Lissenberg, C. J. (2015). Sulfide immiscibility induced by wall-rock assimilation in a fault-guided basaltic feeder system, Franklin Large Igneous Province, Victoria Island (Arctic Canada). *Economic Geology* **110**, 1697–1717.

Hesselbo, S. P. & Coe, A. L. (2000). Jurassic sequences of the Hebrides Basin, Isle of Skye, Scotland. In: Graham, J. R. & Ryan, A. (eds) *Field Trip Guidebook*. International Association of Sedimentologists, pp. 41–58.

Holness, M. B. (1999). Contact metamorphism and anatexis of Torridonian arkose by minor intrusions of the Rum Igneous Complex, Inner Hebrides, Scotland. *Geological Magazine* **136**, 527–542.

Holness, M. B. (2005). Spatial constraints on magma chamber replenishment events from textural observations of cumulates: the Rum Layered Intrusion, Scotland. *Journal of Petrology* **46**, 1585–1601.

Holness, M. B., Sides, R., Prior, D. J., Cheadle, M. J. & Upton, B. G. J. (2012). The peridotite plugs of Rum: Crystal settling and fabric development in magma conduits. *Lithos* **134–135**, 23–40.

Holwell, D. A. & Keays, R. R. (2014). The formation of low-volume, high-tenor magmatic PGE–Au sulfide mineralization in closed systems: Evidence from precious and base metal geochemistry of the Platinova Reef, Skaergaard Intrusion, East Greenland. *Economic Geology* **109**, 387–406.

Holwell, D. A. & McDonald, I. (2006). Petrology, geochemistry and the mechanisms determining the distribution of platinum-group element and base metal sulphide mineralisation in the Platreef at Overysel, northern Bushveld Complex, South Africa. *Mineralium Deposita* **41**, 575–598.

Holwell, D. A. & McDonald, I. (2007). Distribution of platinum-group elements in the Platreef at Overysel, northern

Bushveld Complex: a combined PGM and LA-ICP-MS study. *Contributions to Mineralogy and Petrology* **154**, 171–190.

Holwell, D. A., McDonald, I. & Butler, I. B. (2011). Precious metal enrichment in the Platreef, Bushveld Complex, South Africa: evidence from homogenized magmatic sulfide melt inclusions. *Contributions to Mineralogy and Petrology* **161**, 1011–1026.

Holwell, D. A., Abraham-James, T., Keays, R. R. & Boyce, A. J. (2012). The nature and genesis of marginal Cu–PGE–Au sulphide mineralisation in Paleogene macrodykes of the Kangerlussuaq region, East Greenland. *Mineralium Deposita* **47**, 3–21.

Holwell, D. A., Keays, R. R., Firth, E. A. & Findlay, J. (2014). Geochemistry and mineralogy of platinum group element mineralization in the River Valley Intrusion, Ontario, Canada: A model for early-stage sulfur saturation and multi-stage emplacement and the implications for 'contact-type' Ni–Cu–PGE sulfide mineralization. *Economic Geology* **109**, 689–712.

Hudson, J. D., Coleman, M. L., Barreiro, B. A. & Hollingworth, N. T. J. (2001). Septarian concretions from the Oxford Clay (Jurassic, England, UK): involvement of original marine and multiple external pore fluids. *Sedimentology*. **48**, 507–531.

Hughes, H. S. R., Boyce, A. J., McDonald, I., Davidheiser-Kroll, B., Holwell, D. A., McDonald, A. & Oldroyd, A. (2015). Contrasting mechanisms for crustal sulphur contamination in the British Palaeogene Igneous Province: evidence from dyke and sill complexes on Skye. *Journal of the Geological Society, London*. **172**, 443–458.

Hulbert, L. J., Duke, J. M., Ekstrand, O. R., Scoates, R. F. J., Theriault, R. J., LeCheminant, M. J., Gunn, A. G. & Grinenko, L. N. (1992). Metallogenic and geochemical evolution of cyclic Unit 1, lower Eastern Layered Series, Rhum. In: Foster, R. P. (ed.) *Mineral Deposit Modelling in Relation to Crustal Reservoirs of the Ore-forming Elements*. Institution of Mining and Metallurgy.

Huminicki, M. A. E., Sylvester, P. J., Cabri, L. J., Lesher, C. M. & Tubrett, M. (2005). Quantitative mass balance of platinum group elements in the Kelly Lake Ni–Cu–PGE deposit, Copper Cliff offset, Sudbury. *Economic Geology* **100**, 1631–1646.

Huminicki, M. A. E., Sylvester, P. J., Lastra, R., Cabri, L. J., Evans-Lamswood, D. & Wilton, D. H. C. (2008). First report of platinum-group minerals from a hornblende gabbro dyke in the vicinity of the Southeast Extension Zone of the Voisey's Bay Ni–Cu–Co deposit, Labrador. *Mineralogy and Petrology* **92**, 129–164.

Hutchinson, D. & McDonald, I. (2008). Laser ablation ICP-MS study of platinum-group elements in sulphides from the Platreef at Turfspruit, Northern Limb of the Bushveld Complex, South Africa. *Mineralium Deposita* **43**, 695–711.

Ihlenfeld, C. & Keays, R. R. (2011). Crustal contamination and PGE mineralization in the Platreef, Bushveld Complex, South Africa: evidence for multiple contamination events and transport of magmatic sulphides. *Mineralium Deposita* **46**, 813–832.

Keays, R. R. & Lightfoot, P. C. (2010). Crustal sulfur is required to form magmatic Ni–Cu sulfide deposits: evidence from chalcophile element signatures of Siberian and Deccan Trap basalts. *Mineralium Deposita* **45**, 241–257.

Kerr, A. & Leitch, A. M. (2005). Self-destructive sulfide segregation systems and the formation of high-grade magmatic ore deposits. *Economic Geology* **100**, 311–332.

Kinnaird, T. C., Prave, A. R., Kirkland, C. L., Horstwood, M., Parrish, R. & Batchelor, R. A. (2007). The late Mesoproterozoic–early Neoproterozoic tectonostratigraphic evolution of NW Scotland: the Torridonian revisited. *Journal of the Geological Society, London* **164**, 541–551.

Kullerud, G. & Yoder, H. S. (1959). Pyrite stability relations in the Fe–S system. *Economic Geology* **54**, 533–572.

Labidi, J., Cartigny, P., Birck, J. L., Assayag, N. & Bourrand, J. J. (2012). Determination of multiple sulphur isotopes in glasses: A reappraisal of the MORB δ^{34}S. *Chemical Geology* **334**, 189–198.

Leuthold, J., Blundy, J. D., Holness, M. B. & Sides, R. (2014). Successive episodes of reactive liquid flow through a layered intrusion (Unit 9, Rum Eastern Layered Intrusion, Scotland). *Contributions to Mineralogy and Petrology* **168**, 1–27.

Li, C. Ripley, E. M. 2005. Empirical equations to predict the sulfur content of mafic magmas at sulfide saturation and applications to magmatic sulfide deposits. 40, 218-230. *Mineralium Deposita,* **40**, 218–230.

Li, C., Ripley, E. M., Maier, W. D. & Gomwe, T. E. S. (2002). Olivine and sulfur isotopic compositions of the Uitkomst Ni–Cu sulfide ore-bearing complex, South Africa: evidence for sulfur contamination and multiple magma emplacements. *Chemical Geology* **188**, 149–159.

Lightfoot, P. & Keays, R. R. (2005). Siderophile and chalcophile metal variations in flood basalts from the Siberian Trap, Noril'sk Region: Implications for the origin of the Ni–Cu–PGE sulphide ores. *Economic Geology* **100**, 439–462.

Lightfoot, P. C., Naldrett, A. J. & Hawkesworth, C. J. (1984). The geology and geochemistry of the Waterfall Gorge Section of the Insizwa Complex with particular reference to the origin of the nickel sulphide deposits. *Economic Geology* **79**, 1857–1879.

Lorand, J. –P., Alard, O., Luguet, A. & Keays, R. R. (2003). Sulfur and selenium systematics of the subcontinental lithospheric mantle: Inferences from the Massif Central xenolith suite (France). *Geochimica et Cosmochimica Acta*, **67**, 4137–4151.

Lowry, D. (1991). The genesis of Late Caledonian granitoid-related mineralization in Northern Britain. PhD thesis, University of St Andrews.

Lowry, D., Boyce, A. J., Fallick, A. E., Stephens, W. E. & Grassineau, N. V. (2005). Terrane and basement discrimination in northern Britain using sulphur isotopes and mineralogy of ore deposits. In: McDonald, I., Boyce, A. J., Butler, I. B., Herrington, R. J. & Polya, D. A. (eds) *Mineral Deposits and Earth Evolution. Geological Society, London, Special Publications* **248**, 133–151.

McClurg, J. (1982). Geology and structure of the northern part of the Rhum ultrabasic complex. PhD thesis, University of Edinburgh.

McDonald, I. (2008). Platinum-group element and sulphide mineralogy in ultramafic complexes at western Andriamena, Madagascar. *Applied Earth Science (Transactions Institute of Mining and Metallurgy B)* **117**(**1**), 1–10.

McDonald, I. & Holwell, D. A. (2007). Distribution of platinum-group elements in the Platreef at Overysel, northern Bushveld Complex: a combined PGM and LA-ICP-MS study. *Contributions to Mineralogy and Petrology* **154**, 171–190.

McDonald, I., Holwell, D. A. & Wesley, B. (2009). Assessing the potential involvement of an early magma staging chamber in the generation of the Platreef Ni–Cu–PGE deposit in the northern limb of the Bushveld Complex: a pilot study of the Lower Zone Complex at Zwartfontein. *Transactions of the Institutions of Mining and Metallurgy, Section B* **118**, 5–20.

McDonough, W. F. & Sun, S. s. (1995). The composition of the Earth. *Chemical Geology* **120**, 223–253.

Morton, N. & Hudson, J. D. (1995). Field guide to the Jurassic of the Isles of Raasay and Skye, Inner Hebrides, NW Scotland.

In: Taylor, P. D. (ed.) *Field Geology of the British Jurassic*. Geological Society, 209–280.

Mungall, J. E. & Brenan, J. M. (2014). Partitioning of platinum-group elements and Au between sulfide liquid and basalt and the origins of mantle–crust fractionation of the chalcophile elements. *Geochimica et Cosmochimica Acta* **125**, 265–289.

Mungall, J. E. & Su, S. (2005). Interfacial tension between magmatic sulfide and silicate liquids: Constraints on kinetics of sulfide liquation and sulfide migration through silicate rocks. *Earth and Planetary Science Letters* **234**, 135–149.

Naldrett, A. J. & Fedorenko, V. (1995). Ni–Cu–PGE deposits of the Noril'sk region, Siberia: Their formation in conduits for flood basalt volcanism. *Transactions of the Institution of Mining and Metallurgy* **104**, B18–B36.

Naldrett, A. J., Fedorenko, V. A., Asif, M., Lin, S., Kunilov, V. E., Stekhin, A. I., Lightfoot, P. C. & Gorbachev, N. S. (1996). Controls on the composition of Ni–Cu sulphide deposits as illustrated by those at Noril'sk, Siberia. *Economic Geology* **91**, 751–773.

Naldrett, A. J., Wilson, A., Kinnaird, J. & Chunnett, G. (2009). PGE tenor and metal ratios within and below the Merensky Reef, Bushveld Complex: Implications for its genesis. *Journal of Petrology* **50**, 625–659.

Naldrett, A. J., Kinnaird, J., Wilson, A., Yudovskaya, M. & Chunnett, G. (2011). Genesis of the PGE-enriched Merensky Reef and chromitite seams of the Bushveld Complex. *Reviews in Economic Geology* **17**, 235–296.

Newton, R. J., Bottrell, S. H., Dean, S. P., Hatfield, D. & Raiswell, R. (1995). An evaluation of the use of the chromous chloride reduction method for isotopic analyses of pyrite in rocks and sediment. *Chemical Geology*, **125**, 317–320.

Nielsen, J. K. & Hanken, N. -M. (2002). Description of the chromium reduction method for extraction of pyrite sulphur. University of Tromso.

O'Driscoll, B., Hargraves, R. B., Emeleus, C. H., Troll, V. R., Donaldson, C. H. & Reavy, R. J. (2007). Magmatic lineations inferred from anisotropy of magnetic susceptibility fabrics in Units 8, 9, and 10 of the Rum Eastern Layered Series, NW Scotland. *Lithos* **98**, 27–44.

O'Driscoll, B., Day, J. M. D., Daly, J. S., Walker, R. J. & McDonough, W. F. (2009). Rhenium–osmium isotopes and platinum-group elements in the Rum Layered Suite, Scotland: Implications for Cr–spinel seam formation and the composition of the Iceland mantle anomaly. *Earth and Planetary Science Letters* **286**, 41–51.

O'Driscoll, B., Butcher, A. R. & Latypov, R. (2014). New insights into precious metal enrichment on the Isle of Rum, Scotland. *Geology Today* **30**, 134–141.

Ohmoto, H. & Rye, R. O. (1979). Isotopes of sulphur and carbon. In: Barnes, H. L. (ed.) *Geochemistry of Hydrothermal Deposits*. John Wiley, pp. 509–567.

Parnell, J., Boyce, A. J., Mark, D., Bowden, S. & Spinks, S. (2010). Early oxygenation of the terrestrial environment during the Mesoproterozoic. *Nature* **468**, 290–293.

Parnell, J., Hole, M., Boyce, A. J., Spinks, S. & Bowden, S. (2012). Heavy metal, sex and granites: Crustal differentiation and bioavailability in the mid-Proterozoic. *Geology* **40**, 751–754.

Paterson, S. R., Fowler, T. K., Schmidt, K. L., Yoshinobu, A. S., Yuan, E. S. & Miller, R. B. (1998). Interpreting magmatic fabric patterns in plutons. *Lithos* **44**, 53–82.

Pirrie, D., Power, M. R., Andersen, J. C. Ø. & Butcher, A. R. (2000). Platinum-group mineralization in the Tertiary Igneous Province: new data from Mull and Skye, Scottish Inner Hebrides, UK. *Geological Magazine* **137**, 651–658.

Power, M., Pirrie, D., Andersen, J. C. Ø. & Butcher, A. R. (2000). Stratigraphical distribution of platinum-group minerals in the Eastern Layered Series, Rum, Scotland. *Mineralium Deposita* **35**, 762–775.

Power, M. R., Pirrie, D. & Andersen, J. C. Ø. (2003). Diversity of platinum-group element mineralization styles in the North Atlantic Igneous Province: new evidence from Rum, UK. *Geological Magazine* **140**, 499–512.

Prichard, H. M., Hutchinson, D. & Fisher, P. C. (2004). Petrology and crystallization history of multiphase sulfide droplets in a mafic dike from Uruguay: Implications for the origin of Cu–Ni–PGE sulfide deposits. *Economic Geology* **99**, 365–376.

Prichard, H. M., Knight, R. D., Fisher, P. C., McDonald, I., Zhou, M.-F. & Wang, C. Y. (2013). Distribution of platinum-group elements in magmatic and altered ores in the Jinchuan intrusion, China: an example of selenium remobilization by postmagmatic fluids. *Mineralium Deposita* **48**, 767–786.

Prout, S. J., Andersen, J. C. Ø., Barnes, S.-J. & Power, M. R. (2002). Platinum-group element mineralisation within two mafic/ultramafic intrusions of the British Palaeogene Igneous Province. In: Boudreau, A. E. (ed.) *Proceedings of the 9th International Platinum Symposium, 2002, Billings, Montana, USA*, pp. 383–386.

Raiswell, R., Bottrell, S. H., Al–Biatty, H. J. & Tan, M. M. (1993). The influence of bottom water oxygenation and reactive iron content on sulphur incorporation into bitumens from Jurassic marine shales. *American Journal of Science* **293**, 569–596.

Ripley, E. M., Lightfoot, P. C. & Elswick, E. R. (2003). Sulfur isotopic studies of continental flood basalts in the Noril'sk region: implications for the association between lavas and ore-bearing intrusions. *Geochimica et Cosmochimica Acta* **67**, 2805–2817.

Robertson, J., Ripley, E. M., Barnes, S. J. & Li, C. (2015). Sulfur liberation from country rocks and incorporation in mafic magmas. *Economic Geology* **110**, 1111–1123.

Robertson, J. C., Barnes, S. J. & Metcalfe, G. (2014). Chaotic entrainment can drive sulfide remobilization at low magma flow rates. In: *12th International Platinum Symposium*. Russian Academy of Sciences, pp. 47–48.

Rose, L. A. & Brenan, J. M. (2001). Wetting properties of Fe–Ni–Co–Cu–O–S melts against olivine: Implications for sulfide melt mobility. *Economic Geology* **96**, 145–157.

Saumur, B. M. & Cruden, A. R. (2016). On the emplacement of the Voisey's Bay intrusion (Labrador, Canada). *Geological Society of America Bulletin* 128, 147–168.

Saumur, B. M., Cruden, A. R., Evans-Lamswood, D. M. & Lightfoot, P. C. (2015). Wall-rock structural controls on the genesis of the Voisey's Bay intrusion and its Ni–Cu–Co magmatic sulfide mineralization (Labrador, Canada). *Economic Geology* **110**, 691–711.

Saunders, A. D., Fitton, J. G., Kerr, A. C., Norry, M. J. & Kent, R. W. (1997). The North Atlantic Igneous Province. In: Mahoney, J. J. & Coffin, M. F. (eds) *Large Igneous Provinces: Continental, Oceanic, and Planetary Flood Volcanism*. American Geophysical Union, Geophysical Monograph **100**, 45–93.

Sharman, E. R., Penniston-Dorland, S. C., Kinnaird, J. A., Nex, P. A. M., Brown, M. & Wing, B. A. (2013). Primary origin of marginal Ni–Cu–(PGE) mineralization in layered intrusions: Δ^{33}S evidence from the Platreef, Bushveld, South Africa. *Economic Geology* **108**, 365–377.

Smith, J. W., Holwell, D. A. & McDonald, I. (2014). Precious and base metal geochemistry and mineralogy of the Grasvally Norite–Pyroxenite–Anothosite (GNPA) member, northern Bushveld Complex, South Africa: implications for a multi-stage emplacement. *Mineralium Deposita* **49**, 667–692.

Smith, J. W., Holwell, D. A., McDonald, I. & Boyce, A. J. (2016). The application of S isotopes and S/Se ratio in determining ore-forming processes of magmatic Ni–Cu–PGE sulfide deposits: a cautionary case study from the northern Bushveld Complex. *Ore Geology Reviews* 73, 148–174.

Steel, R. J., Nicholson, R. & Kalander, L. (1975). Triassic sedimentation and palaeogeography in Central Skye. *Scottish Journal of Geology* 11, 1–13.

Stewart, A. D. (2002). *The Later Proterozoic Torridonian Rocks of Scotland: their Sedimentology, Geochemistry and Origin. Geological Society, London, Memoirs 24.*

Torssander, P. (1989). Sulphur isotope ratios of Icelandic rocks. *Contributions to Mineralogy and Petrology* 102, 18–23.

Troll, V. R., Nicoll, G. R., Donaldson, C. H. & Emeleus, H. C. (2008). Dating the onset of volcanism at the Rum Igneous Centre, NW Scotland. *Journal of the Geological Society, London* 165, 651–659.

Tuttle, M. L., Goldhaber, M. B. & Williamson, D. L. (1986). An analytical scheme for determining forms of sulphur in oil shales and associated rocks. *Talanta* 33, 953–961.

Upton, B. G. J. (2004). *Volcanoes and the Making of Scotland.* Dunedin Academic Press.

Upton, B. G. J., Skovgaard, A. C., McClurg, J., Kirstein, L., Cheadles, M., Emeleus, C. H., Wadsworth, W. J. & Fallick, A. E. (2002). Picritic magmas and the Rum ultramafic complex, Scotland. *Geological Magazine* 139, 437–452.

Volker, J. A. & Upton, B. G. J. (1990). The structure and petrogenesis of the Trallval and Ruinsival areas of Rhum ultrabasic complex. *Transactions of the Royal Society of Edinburgh: Earth Sciences* 81, 69–88.

Wadsworth, W. J. (1994). The peridotite plugs of northern Rum. *Scottish Journal of Geology* 30, 167–174.

Wager, L. R., Brown, G. M. & Wadsworth, W. J. (1960). Types of igneous cumulates. *Journal of Petrology* 1, 73–85.

Wagner, T., Boyce, A. & Fallick, A. E. (2002). Laser combustion analysis of δ^{34}S of sulfosalt minerals: determination of the fractionation systematics and some crystal-chemical considerations. *Geochimica et Cosmochimica Acta* 66, 2855–2863.

Yallup, C., Edwards, M. & Turchyn, A. V. (2013). Sulfur degassing due to contact metamorphism during flood basalt eruptions. *Geochimica et Cosmochimica Acta* 120, 263–279.

Zhabina, N. & Volkov, I. (1978). A method of determination of various sulphur compounds in sea sediments and rocks. 3rd International Symposium on Environmental Biogeochemistry. Ann Arbor Science Publications, 735–746.